# Universidad de Concepción

Departamento de Ingeniería Química
Facultad de Ingeniería
Concepción 4070386


# Experimental Determination of Partial Solubility Parameters in Deep Eutectic Solvents

*Thesis submitted in fulfillment of the requirements for the degree of Master of Engineering Sciences*


**Author**
Joaquín Otárola-Sepúlveda

**Supervised by**
Dr. Oscar Valerio

**Committee**
Dr. Gerard Alonso
Dr. Luis Felipe Montoya
Dr.

**Abstract**

This study compares the solubility predictions of the Flory-Huggins-HSP (FH-HSP) model with those of openCOSMO-RS and PC-SAFT, for evaluating the screening capabilities of the Hansen solubility parameters (HSP) using the relative energy difference (RED) parameter. Two deep eutectic solvents, thymol + L-menthol (TM) and thymol + cyclohexanone (TC), and their precursors were investigated. The three models performed reasonably well in predicting the solubility of thymol and L-menthol in organic solvents but showed significant deviations in predicting solid solubility in cyclohexanone. For solubility predictions in DES compared to available experimental data, the root- mean-square logarithmic deviation (RMSLD) values obtained with FH-HSP, openCOSMO-RS, and PC-SAFT were 0.86, 0.27, and 0.93, respectively. Using FH-HSP with HSP obtained from an ideal mixing rule of the parameters of pure compounds resulted in a deviation of 1.13. The screening assessment of the studied DES revealed a 70.4% match rate between the RED parameter and $\ln \gamma_i^{\infty}$, with 6.9% false negatives. Using HSP obtained from the ideal mixing rule resulted in similar scores, with a 68.5% match rate and 10.4% false negatives. The results suggest that the HSP theory can aid DES screening processes by identifying promising DES-solute pairs, thus allowing the targeting of more robust methods of computational resources in smaller sets of compounds.

# Contents

# List of Figures

# List of Tables

# 1. Introduction

## 1.1. Deep eutectic solvents and solubility parameters

Deep eutectic solvents (DESs) are mixtures whose components present enthalpic-driven negative deviations from thermodynamic ideality. These mixtures are characterized by having at least one component that would typically be a solid unsuitable as a solvent [2–4]. The interest in DES arises because these solvents often exhibit convenient properties, such as low costs [5], ease of preparation, low toxicity [6], biodegradability [7], and low volatility [8], among others. However, as these characteristics are not general to all DES and must be evaluated for each system individually [9–13], the key advantage of these solvents lies in their versatility. Since DESs are mixtures, it is possible to tune their physicochemical characteristics by carefully choosing their precursors and adjusting their mole ratios [3].

Among the most investigated applications for DES are extraction and separation processes, for which solubility estimation is crucial. In this sense, a frequently used approach for solvent selection is the solubility parameters theory [14–16]. This theory developed by Hildebrand is based on the empirical concept "like dissolves like" [17]. The base concept is the cohesive energy density ($c_i$), which reflects the molar energy change associated with separating the molecules of a compound $i$ from the condensed phase into an ideal gas [18]. From this, Hildebrand introduced the term solubility parameter ($\delta_i$), as given by Eq. 1.1,

$$\delta_i \equiv c_i^{1/2} = \left(-\frac{E_i}{V_i}\right)^{1/2} \tag{1.1}$$

where $E_i$ is the molar cohesive energy and $V_i$ is the molar volume of the condensed phase of this pure component. The practical implication of Eq. 1.1 is that a suitable solvent could be selected for a target solute according to the likeness of the $\delta_i$. However, this was generally limited to non-polar substances. For improving the applicability,, Hansen extended the solubility parameter concept by considering that $E_i$ can be divided into the sum of three contributions [1] as shown in Eq. 1.2,

$$E_i = E_{\mathrm{d},i} + E_{\mathrm{p},i} + E_{\mathrm{h},i} \tag{1.2}$$

where d, p, and h refer to dispersion, polar and hydrogen bonding contributions, respectively. By dividing the Eq. 1.2 by the molar volume, the total solubility parameter of component $i$ ($\delta_{T,i}$) can be obtained by the sum of the Hansen solubility parameters (HSP) for each contribution, according to Eq. 1.3.

$$\delta_{T,i}^2 = \delta_{\mathrm{d},i}^2 + \delta_{\mathrm{p},i}^2 + \delta_{\mathrm{h},i}^2 \tag{1.3}$$

While the Hildebrand solubility parameter $\delta_i$ is a well-defined thermodynamic quantity (Eq. 1.1), the split into three contributions is an empirical step forward [18]. As a result, even though $\delta_i = \delta_{T,i}$ in practical terms, there must be a distinction between the thermodynamically defined by Eq. 1.1 and the empirically computed by Eq. 1.3.

The HSP for each component $i$ can be represented as a coordinate $(\delta_{d,i}, \delta_{p,i}, \delta_{h,i})$ in the 3D space. In this sense, the degree of interaction between a component $i$ and $j$ is quantified by a "distance" between each coordinate ($R_a$), given by Eq. 1.4.

$$R_a{}^2 = 4(\delta_{d,j} - \delta_{d,i})^2 + (\delta_{p,j} - \delta_{p,i})^2 + (\delta_{h,j} - \delta_{h,i})^2 \tag{1.4}$$

Smaller $R_a$ values translate into higher solubility between compounds. A useful parameter for solvent screening purposes is the relative energy difference (RED) [1] defined as the ratio of $R_a$ and the maximum value where solubility can be expected ($R_0$), as shown in Eq. 1.5.

$$\text{RED} = \frac{R_a}{R_0} \tag{1.5}$$

$0 < \text{RED} < 1$ values mean high affinity, RED = 1 means the limit for solubility, and higher RED values translate into lower affinities.

The RED parameter has been used extensively as a screening tool due to its accessibility, as it can be obtained from experimental data [1, 19, 20] or from group contribution methods [21, 22]. The simplicity of these calculations is attractive and useful for researchers in several fields [23–26].

For a multi-component system, Eq. 1.1 can be expanded in terms of the internal energy change of mixing ($\Delta U$), the molar volume of the mixture ($V$) and the molar fraction of each component ($x_i$), according to Eq. 1.6.

$$\delta^2 = \sum_{i=1}^{n} x_i \delta_i^2 \frac{V_i}{V} - \frac{\Delta U}{V} \tag{1.6}$$

If a thermodynamic ideality is assumed ($\Delta U = 0$), Eq. 1.6 reduces to Eq. 1.7 where the volume fraction of component $i$ ($\phi_i$) is used instead of the volume.

$$\delta_{\text{ideal}}^2 = \sum_{i=1}^{n} \phi_i \delta_i^2 \tag{1.7}$$

However, the linear approach $\delta \approx \sum_{i=1}^{n} \phi_i \delta_i$, rather than Eq. 1.7, is the most common way to estimate the solubility parameters of mixtures. In any case, their applicability to systems that exhibit specific interactions is limited and not well defined, as extensively discussed early by Barton [27] and Hansen [1], and more recently by Panayiotou [28–30]. Despite this, there are several examples in the literature where HSP theory and Eq. 1.7 are used both for ideal and non-ideal systems, including ionic liquids (ILs) and DES [14, 31–38].

Some studies have addressed the validity of Eq. 1.7. For instance, Takebayashi et al. [39] found that Eq. 1.7 may be underestimating the HSP mixtures values of (polar aprotic + protic) systems, as suggested by overestimations of indomethacin solubility in this system and non-ideal deviations of Kamlet-Taft parameters. Vella and Marshall [40] used the Perturbed-Chain Statistical Associating Fluid Theory (PC-SAFT) to estimate the solubility parameters of mixtures. PC-SAFT and Eq. 1.7 gave similar results for several systems, even for non-ideal ones, which agreed well with experimental results. However, noticeable deviations were observed for systems where none of the precursors engaged in hydrogen bonding interactions in their pure state. Bergua et al. [41] used different correlations to calculate the HSP of the thymol + L-menthol system using several physical quantities such as dipole moment and energy of vaporization. They reported that noticeable molar fraction dependence was observed

only for $\delta_p$. The available literature on the subject suggests a scenario where the dependency of the HSP on the molar fraction of DES, and the extent to which this affects HSP solubility predictions for these systems, is not entirely clear.

## 1.2. Motivation and scope

The rationale of this work stems from two main reasons. The first one comes from the question of to what extent the HSP theory can give valuable insights regarding the solubility in DES. As mentioned before, the simplicity of the theory has motivated its use in novel solvents like DES and ILs. The usual form found in the literature to obtain the HSP in DES is by calculating the HSP of the pure compounds, via experimental techniques or group contribution methods, and then using Eq. 1.7 to obtain the mixture's parameters. However, in addition to the fact that the strong intermolecular interactions present in DES complicate the use of the HSP, there is no certainty in whether the resulting HSP from this method accurately represents the interactions present in the actual mixture.

The second reason arises from the fact that, although several studies have been published over the years regarding methodologies for HSP calculation, those are validated, almost invariably, using the data compiled in the Hansen handbook [1]. An important number of values included in this dataset are estimated rather than experimentally determined, and even those have an important degree of uncertainty. This raises doubts about what can be concluded from these error metrics since obtaining a "true" value for any of the HSP appears as a rather uncertain task. Hence, for studying the HSP in DES, an alternative to bypass the need to have reference HSP values for each system is to directly evaluate its ability for making solubility and affinity predictions. For this task, several theoretical tools are available, including well-suited models such as COSMO-RS and PC-SAFT. On the one hand, COSMO-RS (COnductor-like Screening MOdel for Real Solvents) [42, 43] is a statistical thermodynamics theory based on COSMO polarization charge densities that has been extensively applied to investigate solute-solvent interactions. Since it is fully predictive, it has become a frequently used method for screening applications of complex solvents such as ILs and DES [44–47]. On the other hand, PC-SAFT [48, 49] is a widely used equation of state (EoS) to model the thermodynamic properties of fluids, particularly in the context of phase equilibria. PC-SAFT has proven to be an effective tool for modeling the solubility of different compounds in various solvents [50, 51], including DES [52–54].

In this work, two binary mixtures, thymol + L-menthol (TM) and thymol + cyclohexanone (TC), were prepared to determine the HSP using two different experimental approaches. The first one uses the sphere fitting method, which takes as input binary information of "good" and "bad" solvents with known HSP. The second approach uses intrinsic viscosity to quantify the interactions between DES in different solvents, and then from this data extract the HSP of each DES using different methods. The recent open-source implementation of COSMO-RS reported by Gerlach et al. [55] (openCOSMO-RS) and PC-SAFT EoS [48, 49] were used to calculate the activity coefficients of these DES with several compounds of different characteristics in order to evaluate the solubility estimations of the HSP theory. Given that the HSP theory has been applied to systems that go well beyond the constraints for which it was originally developed, the purpose of this study is to assess the scope of the HSP theory as applied to DES by comparing common experimental methods for HSP determination with robust computational tools.

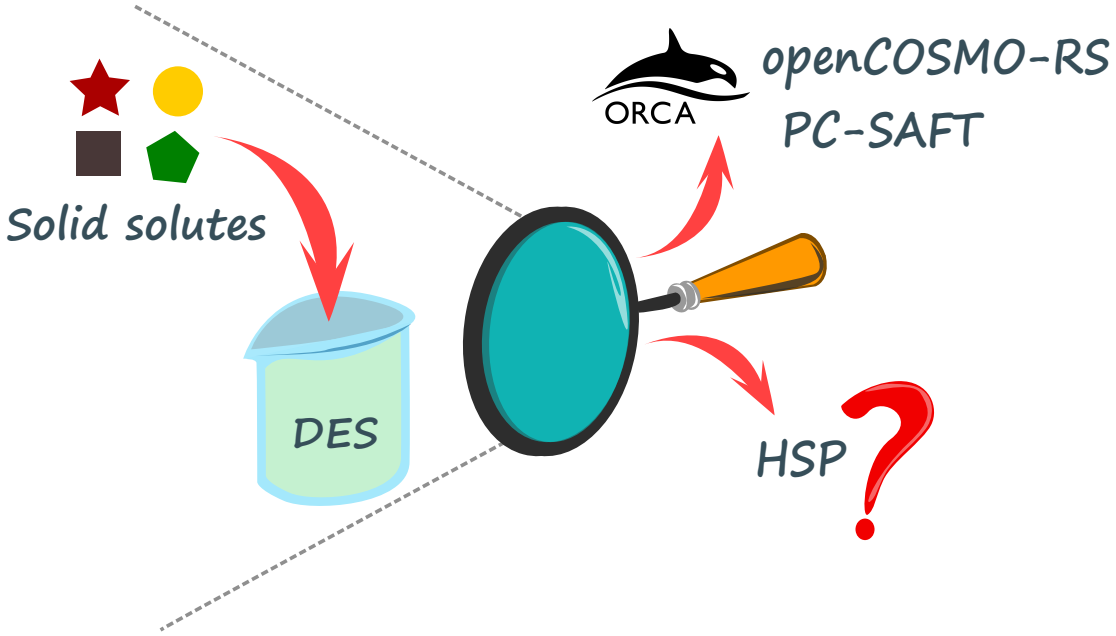


Figure 1.1.: Graphical representation of the aim of this study. The ability of the HSP theory to model the solubility of solids in DES is evaluated by comparing it with openCOSMO-RS and PC-SAFT.

## 1.3. Hypothesis and objectives

### 1.3.1. Hypothesis

1. Hansen solubility parameters allow for the calculation of the solubility of solid solutes in deep eutectic solvents.

2. Intrinsic viscosity allows the determination of Hansen solubility parameters values for deep eutectic solvents, which can be used to predict the solubility of these systems with solid solutes.

3. The Hansen solubility parameters of a deep eutectic solvents deviate from linear behavior with respect to composition.

### 1.3.2. Objectives

#### General objective

Determine experimentally the solubility parameters of different DES, and study their potential estimation from their pure components.

#### Specific objectives

1. To study the predictive ability of Hansen solubility parameters in terms of solubility of solid solutes in deep eutectic solvents.

2. To compare the Hansen solubility parameters obtained in deep eutectic solvents using the solubility test technique with those obtained from intrinsic viscosity measurements.

3. Evaluate whether the ideal mixing rule used to estimate the solubility parameters of mixtures applies to deep eutectic solvents.

4. To explore the possibility of establishing a mixing rule, based on preferential solvation theory, to predict the solubility parameters of binary DES from their pure components.

5. To compare the performance of the Hansen solubility parameters theory for calculating the solubility of solid solutes in deep eutectic solvents with COSMO-RS and PC-SAFT models.

6. To evaluate the capacity of Hansen solubility parameters theory for screening applications of solid solutes in deep eutectic solvents.

# 2. Methods and materials

## 2.1. Chemicals

The chemicals used for DES preparation is included in Table 2.1, along with the specifications reported by the provider. The solvents used for the solubility test are attached to Table A.1. All the compounds were used without purification.

Table 2.1.: Specifications of the compounds used in this work for DES preparation, along with their molar mass ($M$), CAS number, and supplier.

| Chemical name | $M$ / g · mol$^{-1}$ | CAS | Supplier | Purity / wt.% |
|---|---|---|---|---|
| Thymol | 150.218 | 89-83-8 | Sigma Aldrich | ≥ 98.5 |
| L-Menthol | 156.265 | 2216-51-5 | TCI Chemicals | ≥ 99.0 |
| Cyclohexanone | 98.143 | 108-94-1 | Sigma Aldrich | ≥ 99.0 |

## 2.2. Mixtures preparation

The DES used in this work were prepared gravimetrically at different compositions using an analytical balance (Practicum 224-1s Sartorius, Germany) in different proportions. The mixtures were heated under stirring at 323.15 K until a homogeneous and clear liquid was formed. After cooling at room temperature, only the samples that remained a stable liquid were selected for solubility parameter determination. The water content of the mixtures was measured using a Karl Fischer Coulometer (831 KF Metrohm, Switzerland) and a Volumetric Karl Fischer (870 KF Titrino plus Metrohm, Switzerland). Detailed information on the prepared DES is presented in Table 2.2.

## 2.3. Modeling

### 2.3.1. Hansen solubility parameters (HSP)

The HSP of the pure compounds selected in this work were obtained from the dataset reported by Díaz de los Ríos and Hernández Ramos [56]. HSP were estimated using the group contribution method described by Mathieu [57] for compounds not included in this dataset. In order to calculate the HSP for DES, two experimental approaches were used. In the first approach (HSP1), each DES sample was dissolved in 20 solvents using 0.5 mL of DES in 7 mL of solvent, shaken for 24 h at 160 rpm and 298.15 K, and left to settle for 1 h before interpreting the results. Each solvent was rated as "good" or "bad" based on its ability to dissolve the solute completely or not, respectively, by visual inspection. Then, the Excel Sheet developed

Table 2.2.: Specifications of the studied DES. $x_{thy}$ is the mole fraction of thymol, $M_{DES}$ is the molar mass, and $\phi_{thy}$ is the volume fraction of thymol.

| DES | $x_{thy}$ / mol · mol$^{-1}$ | $M_{DES}$ / g · mol$^{-1}$ | $\phi^a_{thy}$ / mL · mL$^{-1}$ | Water content / ppm |
|---|---|---|---|---|
| Thymol + L-Menthol (TM) | 0.3303 | 154.27 | 0.3042 | 118.5 |
| | 0.4171 | 153.75 | 0.3882 | 1004.8 |
| | 0.4978 | 153.26 | 0.4678 | 117.7 |
| | 0.5905 | 152.70 | 0.5611 | 548.5 |
| | 0.6818 | 152.14 | 0.6552 | 64.4 |
| Thymol + Cyclohexanone (TC) | 0.0772 | 102.16 | 0.1117 | 5048 |
| | 0.1513 | 106.02 | 0.2112 | 5549 |
| | 0.2844 | 112.95 | 0.3738 | 4324 |
| | 0.6145 | 130.14 | 0.7054 | 4655 |
| | 0.7833 | 138.93 | 0.8445 | 5026 |

[a] Calculated using densities reported by the provider of 0.965 g·mL$^{-1}$, 0.890 g·mL$^{-1}$, and 0.947 g·mL$^{-1}$ for thymol, L-menthol, and cyclohexanone, respectively.

by Díaz de los Ríos and Hernández Ramos [56] was utilized, which takes previous binary classification as an input to determine the best coordinates for the center of the Hansen sphere and the radius $R_0$ for each DES, while considering errors caused by good and bad solvent mismatches.

The second experimental approach uses intrinsic viscosity measurements ($[\eta_i]$) of diluted DES samples in 8 organic solvents, which are included in Tables S2 and S3. These dilutions were prepared by mixing 0.25 mL of DES and 5 mL of solvent. The dynamic viscosities of the pure solvent ($\eta_0$) and DES+solvent mixture ($\eta$) were measured using an Anton Paar Lovis 2000ME microviscometer (Graz, Austria) at 298.15 K. Then, the intrinsic viscosity was calculated using a single concentration measurement using the Solomon-Ciută equation [58], as shown in Eq. 2.1,

$$[\eta_i] = \frac{\sqrt{2\left[\frac{\eta}{\eta_0} - 1 - \ln\left(\frac{\eta}{\eta_0}\right)\right]}}{C} \tag{2.1}$$

where $C$ is the concentration of the DES in the solvent in g/100 mL.

Intrinsic viscosity data has been successfully used for calculating solubility parameters of molecules smaller than polymers, such as ILs and *p*-xylene oxidation derivatives. However, to the best of the authors' knowledge, Eq. 2.1 has not been previously used for DESs. A brief discussion of the applicability of Eq. 8 for these systems is included in .

To calculate the HSP from viscosity data, three calculation methods were used for comparison. The first method, proposed by Segarceanu and Leca [59] (HSP2-S), uses the normalized intrinsic viscosity ($[\eta'_i] = [\eta_i]/[\eta_{max}]$) and the HSP of each solvent used ($\delta_{d,i}$, $\delta_{p,i}$ and $\delta_{h,i}$) to calculate the HSP of each DES using Eq. 2.2.

$$\delta_x = \frac{\sum\left(\delta_{x,i} \cdot \left[\eta'_i\right]\right)}{\sum\left[\eta'_i\right]} \;\; ; \;\; x = \mathrm{d, p, h} \tag{2.2}$$

The second method is the one proposed by Bustamante et al. [60] (HSP2-B). This method fits the intrinsic viscosity measurements of each DES sample in the different solvents using the least-squares method with 7 constants ($C_0$-$C_6$), according to Eq. 2.3.

$$\ln[\eta_i] = C_0 + C_1\delta_{\mathrm{d}i} + C_2\delta_{\mathrm{d}i}^2 + C_3\delta_{\mathrm{p}i} + C_4\delta_{\mathrm{p}i}^2 + C_5\delta_{\mathrm{h}i} + C_6\delta_{\mathrm{h}i}^2 \tag{2.3}$$

Then, the HSP of each DES are calculated using these constants by Eq. 2.4.

$$\delta_{\mathrm{d}} = -\left(\frac{C_1}{2C_2}\right) \; ; \; \delta_{\mathrm{p}} = -\left(\frac{C_3}{2C_4}\right) \; ; \; \delta_{\mathrm{h}} = -\left(\frac{C_5}{2C_6}\right) \tag{2.4}$$

The last method computes the functional solubility parameters (FSP) of each DES sample. The central assumption of this method is that the intrinsic viscosity of the DES in each solvent gives a quantitative measure of the affinity between both compounds, allowing to construct a density function which has for domain the 3D-space formed by the contributions ($\delta_{\mathrm{d}}$, $\delta_{\mathrm{p}}$, $\delta_{\mathrm{h}}$), and the $[\eta_i]$ values as the range. The density function and FSP calculation were done using the MATLAB-FreeFEM++ workflow available in the original work of Howell et al. [61], to which the reader is referred for details of the method.

Regardless of the method used to obtain the HSP, the activity coefficient for component $i$ ($\gamma_i$) can be calculated using the extended Hansen model combined with the Flory-Huggins entropy correction [62, 63], according to Eq. 2.5,

$$\ln \gamma_i = \ln \frac{\phi_i}{x_i} + 1 - \frac{\phi_i}{x_i} + \chi_{ij}\phi_j^2 \tag{2.5}$$

where $\chi_{ij}$ is the Flory-Huggins interaction parameter between components $i$ and $j$. This parameter can be expressed in terms of HSP according to Eq.2.6,

$$\chi_{ij} = \alpha \frac{V_i}{4RT} R_{\mathrm{a}}^2 \tag{2.6}$$

where $R$ is the ideal gas constant, $T$ is the absolute temperature of the system and the parameter $\alpha$ is set equal to 0.6 as suggested by 62.

### 2.3.2. COSMO-RS

The COSMO-RS theory assumes that the thermodynamics of a system composed of chemical compounds can be described by the thermodynamics of an ensemble of pairwise interacting surface segments. The interactions between these segments can be set to be a function of various descriptors, with the main one being the screening charge $\sigma$. These charges are calculated using quantum chemistry, particularly density functional theory (DFT). To obtain the $\sigma$ values for each segment, a molecule is first represented as a cavity, which is a smoothed, continuum surface that covers the molecule. This cavity is embedded in a hypothetical perfectly conducting medium (infinite permittivity). Then, the geometry of the molecule is optimized in several steps, and the screened charge generated in each of the segments of the cavity is calculated. Using this information, the $\sigma$-profile, which is the actual input for the statistical thermodynamics calculations of the method, can be computed. The $\sigma$-profile is a histogram of the screening charge of the molecules, i.e. the probability of finding a segment with a screened charge $\sigma$ [64].

Once the $\sigma$-profile is obtained, the calculations regarding the surface contact interactions are conducted. The fraction of a segment type $I$ in a segment mixture can be expressed as,

$$X^I = \frac{\sum_i x_i n_i^I}{\sum_i \sum_J x_i n_i^J} \tag{2.7}$$

where $n_i^I$ is the number of segments of type $I$ on a molecule of type $i$, and $\sum_J$ sums over all the types of segments. The activity coefficient of each segment is given by the expression,

$$\Gamma^I = \frac{1}{\sum_J X^J \Gamma^J \tau_{IJ}} \tag{2.8}$$

where the interaction parameter $\tau_{IJ}$ can be defined as,

$$\tau_{IJ} = \exp\left(\frac{-G_{IJ}^{int}}{RT}\right) \tag{2.9}$$

where $-G_{IJ}^{int}$ is the interaction free energy of a contact between segments $I$ and $J$. This interaction free energy is specified as a function of the set of segment type descriptors. Eq.2.8 corresponds to the general COSMOSPACE equations and can be solved iteratively by simple repeated substitution [65]. Once these equations have been solved, it is possible to calculate the residual part of the activity coefficient at a given composition with respect to the pure compound $i$ as,

$$\ln \gamma_i^{\text{res}} = \sum_I \frac{q_i}{a_{\text{eff}}} (\ln \Gamma^I - \ln \Gamma_i^I) \tag{2.10}$$

where $q_i$ is the total surface area of molecule $i$, $a_{\text{eff}}$ is the size of the surface segments, and $\Gamma_i^I$ is the activity coefficient of segment $I$ in an ensemble of pure compound $i$. The combinatorial contribution is calculated using the Staverman-Guggenheim expression [66],

$$\ln \gamma_i^{\text{comb}} = \ln \frac{\phi_i}{x_i} + 1 - \frac{\phi_i}{x_i} - 0.5 z \frac{q_i}{q} \left(\ln \frac{\phi_i}{\theta_i} + 1 - \frac{\phi_i}{\theta_i}\right) \tag{2.11}$$

$$\frac{\phi_i}{x_i} = \frac{V_i}{\sum_j x_j V_j} \tag{2.12}$$

$$\frac{\theta_i}{x_i} = \frac{q_i}{\sum_j x_j q_j} \tag{2.13}$$

where $z$ is the coordination number and is typically chosen to be equal to 10. $q_i$ and $V_i$ are considered to be the volume and surface area of the cavity of molecule $i$, respectively. $q$ is a universal parameter of the model.

Then, the activity coefficient of component $i$ is calculated according to Eq. 2.14,

$$\ln \gamma_i = \ln \gamma_i^{\text{res}} + \ln \gamma_i^{\text{comb}} \tag{2.14}$$

To test the accuracy of the calculations, in this work the infinite dilution activity coefficients ($\gamma_i^{\infty}$) were calculated using openCOSMO-RS and compared to both experimental values and predictions from the COSMOthermX C30_1705 software, as reported by Brouwer and Schuur [67].

The COSMO-RS calculations were carried out using the open-source implementation developed by Gerlach et al. [55] (openCOSMO-RS). The geometries of all the investigated molecules were optimized using the RDKit/ORCA workflow [55], which acts as a "sieve", filtering conformers based on energy and re-optimizing them with more robust calculations. First, RDKit is used to generate a set of initial conformers of the target molecule using the respective SMILES, utilizing the distance geometry approach [68, 69] and MMFF94 force field. Conformers are filtered and optimized using ORCA [70–72] in successive steps, with a final COSMO single point calculation at DFT/BP86/def2-TZVPD level. The generated .orcacosmo files are used as input for the subsequent COSMO-RS calculations, which are carried out using Python. The reader is referred to the original work for the detailed methodology [55].

### 2.3.3. PC-SAFT

PC-SAFT is an equation of state developed by Gross and Sadowski [48, 49], which has been widely used in the modeling of thermodynamic properties of fluids. The core of the PC-SAFT model is the residual Helmholtz energy of the fluid ($a_{\text{res}}$), which is expressed as a sum of different contributions. These include a hard chain as reference fluid ($a_{\text{hc}}$), dispersion interactions ($a_{\text{disp}}$), and association contributions ($a_{assoc}$), as shown in Eq. 2.15.

$$a_{\text{res}} = a_{\text{hc}} + a_{\text{disp}} + a_{\text{assoc}} \tag{2.15}$$

At least three parameters are necessary to define a molecule with the PC-SAFT framework properly. These parameters include the number of segments ($m_s$), the segment diameter ($\sigma$), and the dispersion energy between segments ($\varepsilon$). For molecules with association sites, two additional parameters are required, including the association volume ($\kappa^{AB}$) and the association energy ($\varepsilon^{AB}$). Although these parameters can be adjusted to fit specific properties, improving the accuracy of the predictions [73], the PC-SAFT EoS was used in this work in a predictive way using the COSMO computations as recently shown by Mahmoudabadi and Pazuki [74] (Table E.1). In this approach, association volumes are fixed at $\kappa^{AB} = 0.02$, and the association scheme 2B was assumed for associating compounds.

Furthermore, the respective mixing rules of the model were used to extend it to mixtures without the need for any binary interaction parameters, making PC-SAFT as fully predictive as COSMO-RS in this work.

The activity coefficient for a component *i* in the PC-SAFT model can be obtained using the fugacity coefficient in the mixture ($\hat{\phi}_i$) and in the pure state at the same system temperature and pressure ($\phi_{i,\text{pure}}$), as is shown in Eq. 2.16.

$$\ln \gamma_i = \ln \hat{\phi}_i - \ln \phi_{i,\text{pure}} \tag{2.16}$$

In the previous equation, the fugacity coefficients were calculated using Eq. 2.17,

$$\begin{aligned} \ln \hat{\phi}_i = a_{\text{res}} + (Z-1) + \left(\frac{\partial a_{\text{res}}}{\partial x_i}\right)_{T,v,x_{k\neq i}} \\ - \sum_{j=1}^{N} \left[ x_j \left(\frac{\partial a_{\text{res}}}{\partial x_j}\right)_{T,v,x_{k\neq j}} \right] - \ln Z \end{aligned} \tag{2.17}$$

where the compressibility factor ($Z$) is calculated by using Eq. 2.18.

$$Z = 1 + \rho \left( \frac{\partial a_{\text{res}}}{\partial \rho} \right)_{T,x_k} \tag{2.18}$$

### 2.3.4. Solid-liquid equilibrium

The mole fraction solubilities of a solid solute $i$ in a solvent, $x_i$, were calculated for all the different activity coefficient models under the assumption of a pure solid phase by using Eq. 2.19 [75],

$$\begin{aligned} \ln(x_i \gamma_i) = & \frac{\Delta_m H_i}{R} \left( \frac{1}{T_{m,i}} - \frac{1}{T} \right) \\ & + \frac{\Delta_m C_{p,i}}{R} \left( \frac{T_{m,i}}{T} - \ln \frac{T_{m,i}}{T} - 1 \right) \end{aligned} \tag{2.19}$$

where $\Delta_m H_i$ is its melting enthalpy, $T_{m,i}$ is its melting temperature, and $\Delta_m C_{p,i}$ is its heat capacity change upon melting condition. Generally, the heat capacity term is negligible compared with the enthalpic term [75, 76], obtaining Eq. 2.20.

$$\ln(x_i \gamma_i) = \frac{\Delta_m H_i}{R} \left( \frac{1}{T_{m,i}} - \frac{1}{T} \right) \tag{2.20}$$

The melting properties of each compound are listed in Table F.1.

# 3. Results

This section is organized as follows. Firstly, in Sec. 3.1, we discuss the non-ideality of the eutectic systems under study, with a particular focus on TC since this specific mixture has not been previously reported in the literature.

Next, in Sec. 3.2, we assess the capabilities of the HSP theory when applied to the pure substances used in the formation of DES, namely thymol, L-menthol, and cyclohexanone. This assessment involves both quantitative and qualitative predictions, as we compare the HSP theory to COSMO-RS and the predictive PC-SAFT. Solubility predictions of thymol and L-menthol are evaluated using these as solutes in several common organic solvents, since both are solids at room temperature. As cyclohexanone is liquid at room temperature, HSP are evaluated by estimating the solubility of solid solutes in it. Although mixing these two approaches (using some substances in question as solutes and other as solvent) is not ideal, evaluating the HSP model using cyclohexanone as a solute was not possible, since this model is not aimed for liquid-liquid calculations. Moreover, cyclohexanone melting point is very low (around -31°C), so although there are correlations to extrapolate the HSP values to other temperatures, such a lower temperature would escape the capabilities of the model.

Subsequently, in Sec. 3.3, we present the HSP obtained using different methods, i.e., HSP1, HSP2-S, HSP2-B, and FSP. Additionally, we evaluate these HSP in terms of their capabilities for solubility predictions. Due to the scarcity of experimental solubility data in systems like TM and TC, each model is also compared using a larger set of solid solutes that, although lack experimental data, allow to assess the predictions in a more general way.

The results are presented in the order shown (i.e. pure substances first, then DES) in order to observe the limitations of the model in a more systematic manner.

## 3.1. Non-ideality of the mixtures

A common approach for determining whether a eutectic mixture is a DES is to measure the SLE and check for negative deviations from thermodynamic ideality. TM is a well-studied system, and its equilibrium data have been reported in the literature [77, 78], demonstrating its non-ideality [79] and thus qualifying it as a DES. Conversely, to the best of our knowledge, the SLE of TC has not been reported in the literature. Nevertheless, the non-ideality of the system can be demonstrated using a qualitative approach. For that, various TC samples at different concentrations were kept at approximately 263 K for seven days. The results revealed that all samples analyzed maintained homogeneity as liquids, indicating that the SLE of TC has a negative deviation from ideality, as is shown in Fig. S1. For example, the ideal solubility line predicts that the sample containing $x_{\text{thy}} = 0.7$ should precipitate ideally at around 308.4 K, which is 45 K higher than the temperature at which it was observed as a homogeneous liquid. Also, Fig. S1 demonstrates that the openCOSMO-RS prediction aligns well with the experimental observations, showing liquidus lines with a sharp slope. The observed shape is common among eutectic mixtures that form cocrystals [78, 80, 81], which is

reflected in the segmented lines of the SLE diagram due to the different melting properties of each cocrystal. It is most likely that the openCOSMO-RS prediction shown is only valid for the range where only pure crystals precipitate from the mixture. From these results, it can be concluded that TC is a DES.

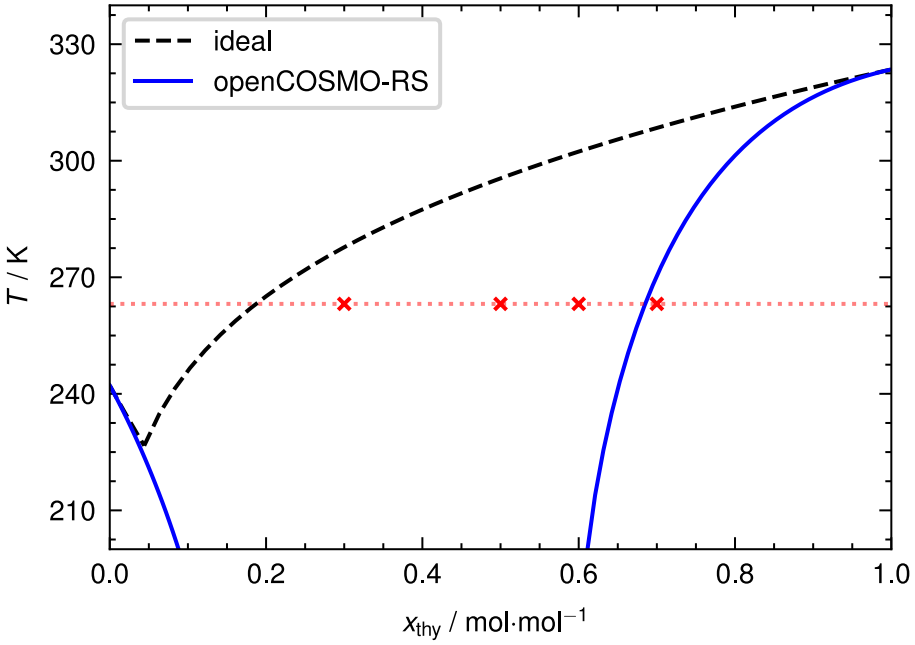


Figure 3.1.: Ideal SLE diagram for thymol + cyclohexanone, along with the predictions using openCOSMO-RS. Red points are DES compositions observed to remain a stable liquid at the respective temperature. Melting properties of thymol are included in Table F.1, while melting properties of cyclohexanone were obtained from literature [82] ($T_m$ = 245.2 K and $\Delta_m H$ = 1.33 kJ·mol$^{-1}$).

## 3.2. HSP of pure compounds

Although several methods exist for calculating HSP, including recent advancements [83–85], in several applications the critical test for these parameters is their effectiveness in screening processes. To assess this, the predictive capabilities of HSP were evaluated quantitatively by calculating mole fraction solubility and qualitatively by classifying solute-solvent pairs as "good" or "bad" on its ability to dissolve the solute by visual inspection.

The precursors of the studied DES were selected to evaluate the HSP approach to solubility for systems of pure solid solutes in pure solvents. Experimental solubility data for L-menthol and thymol in 7 organic solvents, as well as the solubility data of 8 solid solutes in cyclohexanone, were collected from the literature. These collected data were then compared to predictions obtained using openCOSMO-RS, FH-HSP, and PC-SAFT. Literature data are summarized in Table G.1. To determine the accuracy of the solubility predictions obtained from each model, the root-mean-square logarithmic deviation (RMSLD) was used as a met-

ric, which is calculated using Eq. 3.1,

$$\text{RMSLD} = \sqrt{\frac{1}{N}\sum_{i=1}^{N}(\log_{10} x_i^{\text{pred}} - \log_{10} x_i^{\text{exp}})^2} \tag{3.1}$$

where $N$ represents the number of experimental data points of a solute $i$ and the superscripts "pred" and "exp" refer to predicted and experimental solubility data, respectively.

As observed in Fig. 3.2, the three models give a reasonable performance for the solubility of thymol and L-menthol, with RMSLD < 0.13 log units. As shown in Fig. 3.2a, worse predictions are obtained for the solubility of solid solutes in cyclohexanone, with RMSLDs of 0.63, 0.46 and 0.55 log units for openCOSMO-RS, FH-HSP and PC-SAFT, respectively. For the majority of cyclohexanone data, and for some thymol and L-menthol data points, it is observed that FH-HSP has a tendency to underestimate solubilities by overestimating $\gamma_i$, whereas openCOSMO-RS and PC-SAFT tend to overestimate solubilities by underestimating $\gamma_i$. For FH-HSP, this can be understood considering that the $R_a$ term does not allow negative values, being a positive contribution to Eq. 2.5 regardless of the system. For the openCOSMO-RS model, overestimations in the solid solubilities have been previously reported in the literature [73]. One possible explanation comes from inaccuracies in the estimation of the hydrogen bonding free energy contribution, as has been observed in other works [86]. There are some ways to improve this behavior. For example, although not used in this work, openCOSMO-RS allows the use of element scaling parameters, which weigh the strength of the interactions between segments according to the respective element. Parametrization for the use of these descriptors may improve the predictions.

Regarding PC-SAFT, the deviations observed in Fig. 3.2 can be rationalized by considering that PC-SAFT was employed in a fully predictive manner. In this approach, the parameters of the pure substances were obtained from COSMO calculations using ORCA, and no binary parameters were fitted. It is known that the accuracy of PC-SAFT can be improved by incorporating parameters that are fitted to liquid properties such as density and vapor pressure. These parameters provide a more precise characterization of the solvent, which, in turn, can help improve the prediction of solid solubilities. However, the parametrization strategy used for liquid solvents cannot be applied to solutes, which have low volatility and high melting points. Instead, it is necessary to use experimental solubility data in particular pure solvents, which has been shown to give accurate results [50, 87, 88]. Although fitting binary parameters would be the standard way to proceed in this case, it was not within the scope of this study, since the aim was to evaluate the three models in a predictive fashion, avoiding the use of extra adjustable parameters to the experimental data so as to prevent overfitting and maintain a comparative balance between the models. For instance, the FH-HSP model has also been shown capable of fitting the solubility of APIs in several solvents, but by letting the HSP of the API and another two parameters as adjustable ones [39].

For the qualitative evaluation of the HSP approach, the RED parameter was compared to $\ln \gamma_i^{\infty}$ obtained using openCOSMO-RS. This parameter has been successfully used as an indicator in solvent screening applications [45, 89], were decreasing negative values of $\ln \gamma_i^{\infty}$ correspond to higher solute-solvent interactions, analogous to smaller values of RED. This limit can be understood considering that the activity coefficient can be expressed as,

$$\ln \gamma_i = \frac{\mu_i - \mu_i^0}{RT} \tag{3.2}$$

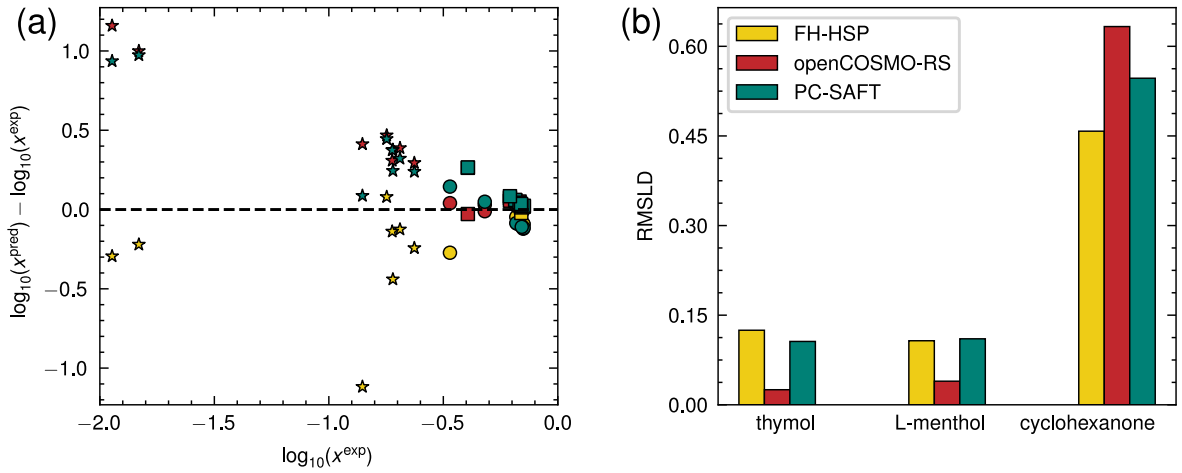


Figure 3.2.: Deviations obtained for each model in solubility prediction in pure solvents. (a) Relationship between the prediction error with experimental solubilities close to 298.2 K (see Table G.1). Each point corresponds to solute-solvent pairs which include thymol (○), L-menthol (□), and cyclohexanone (☆); (b) RMSLD of each model for thymol, L-menthol, and cyclohexanone. The experimental data used from the literature is included in Table G.1.

where $\mu_i$ and $\mu_i^0$ are the chemical potential of solute $i$ in the mixture and in a system with $x_i = 1$, respectively. Negative values for $\ln \gamma_i$ would mean that introducing a molecule of $i$ into the mixture is energetically more favorable than introducing it in the pure at these conditions. This means that the solute molecule $i$ will have a tendency to undergo change into the solvent. This limit is somehow analogous to the limit of RED = 1, which means that the solvent is just entering the "solubility region" of a given solute. The aim was to determine how closely these two criteria corresponded.

The results of the qualitative evaluation of HSP for pure solvents are presented in Fig. 3.3. The solute-solvent pairs evaluated and the respective HSP are reported in the Excel file included in the Supporting Information. The plane is divided into four quadrants, representing zones with matches (I and III) and mismatches (II and IV) between $\ln \gamma_i^\infty$ and RED. Out of the 2204 pairs that were evaluated, 66.1% of the points correspond to matches between RED and $\ln \gamma_i^\infty$. Quadrant II correspond to 21.7%, and quadrant IV to 12.2%. It is worth noting that while both quadrant II and IV represent mismatches, quadrant IV is less desirable because it corresponds to false negatives, i.e. solvents that RED would screen as "bad" for the given solute, contrary to openCOSMO-RS prediction. As a result, quadrant IV points should be treated with caution, as without experimental corroboration is not possible to know whether RED or $\ln \gamma_i^\infty$ are correctly describing solute-solvent affinity. False positives, which are represented by datapoints in quadrant II, are generally less harmful to the screening process than false negatives. This is because the RED parameter is often used as an initial filter, and further refinement of the screening process can be performed using more rigorous tools in subsequent stages. From a practical point of view, RED is able to reduce the initial dataset to around half (1100 pairs), from which 56.6% (622 pairs) are true positives, which is a reasonable performance considering the simplicity of the calculations.

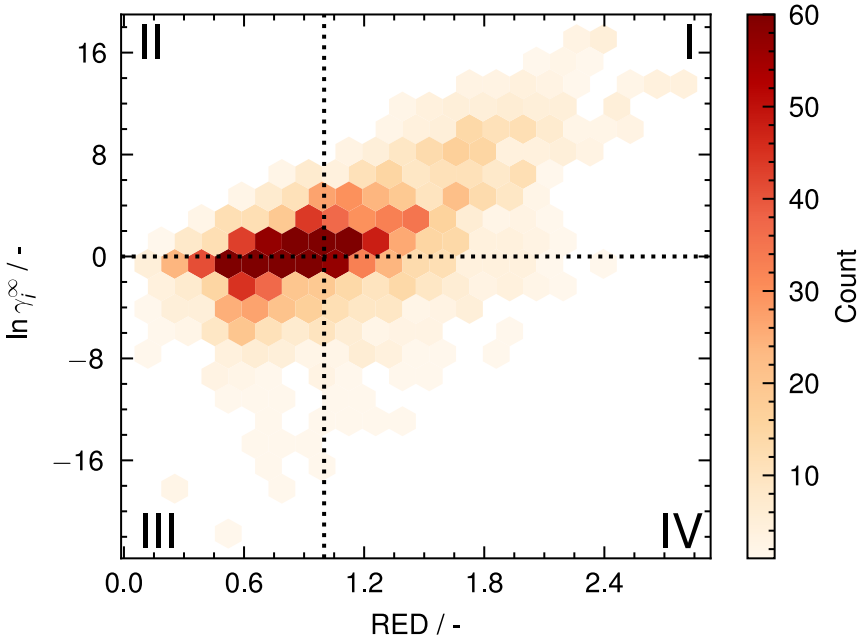


Figure 3.3.: Hexbin plot showing the relationship between predicted $\ln \gamma_i^\infty$ using openCOSMO-RS and the RED parameter between a pure solid solute $i$ and a pure solvent at 298.15 K. The color intensity represents the number of points in each hexagon. The plot is divided into four quadrants, representing the matches (I and III) and mismatches (II and IV) between both screening parameters.

## 3.3. HSP of DES

### 3.3.1. HSP results

The measured solubility parameters for TM and TC at each HBA:HBD ratio are reported in Table H.1, and the intrinsic viscosity calculations are included in Tables C.2 and C.3. One important objective of this work was to investigate the dependence of HSP with mole fraction in DES. Fig. 3.4 shows the HSP obtained for TM and TC as a function of $x_{\text{thy}}$ for each system. Two immediate observations can be made from this plot. First, each solubility parameter exhibits a deviation from the ideal prediction (Eq. 1.7) in both systems, with the highest deviation observed in $\delta_{\text{p}}$. Second, the methods (HSP1, HSP2S, HSP2-B, and FSP) used for computing the HSP do not reveal a dependence of these parameters with mole fraction. Both observations are discussed in the following.

The HSP values obtained with each method show a similar tendency, except for the HSP2-B method. It shows a significant deviation from the general trend in the calculated values (Fig. 3.4b, 3.4c, and 3.4f). Moreover, the HSP2-B method resulted in negative HSP values for two TC samples ($x_{\text{thy}}$ = 0.0772 and 0.7833), which were left out of the plot. To investigate this, a bootstrapping was performed for HSP2-B and HSP2-S for comparison. Bootstrapping works by randomly resampling the experimental data, generating the called “bootstrap samples”, with which the target indicator (in this case the respective HSP) can be recalculated (see the Supporting Information for further details on bootstrapping). It was found that minor errors

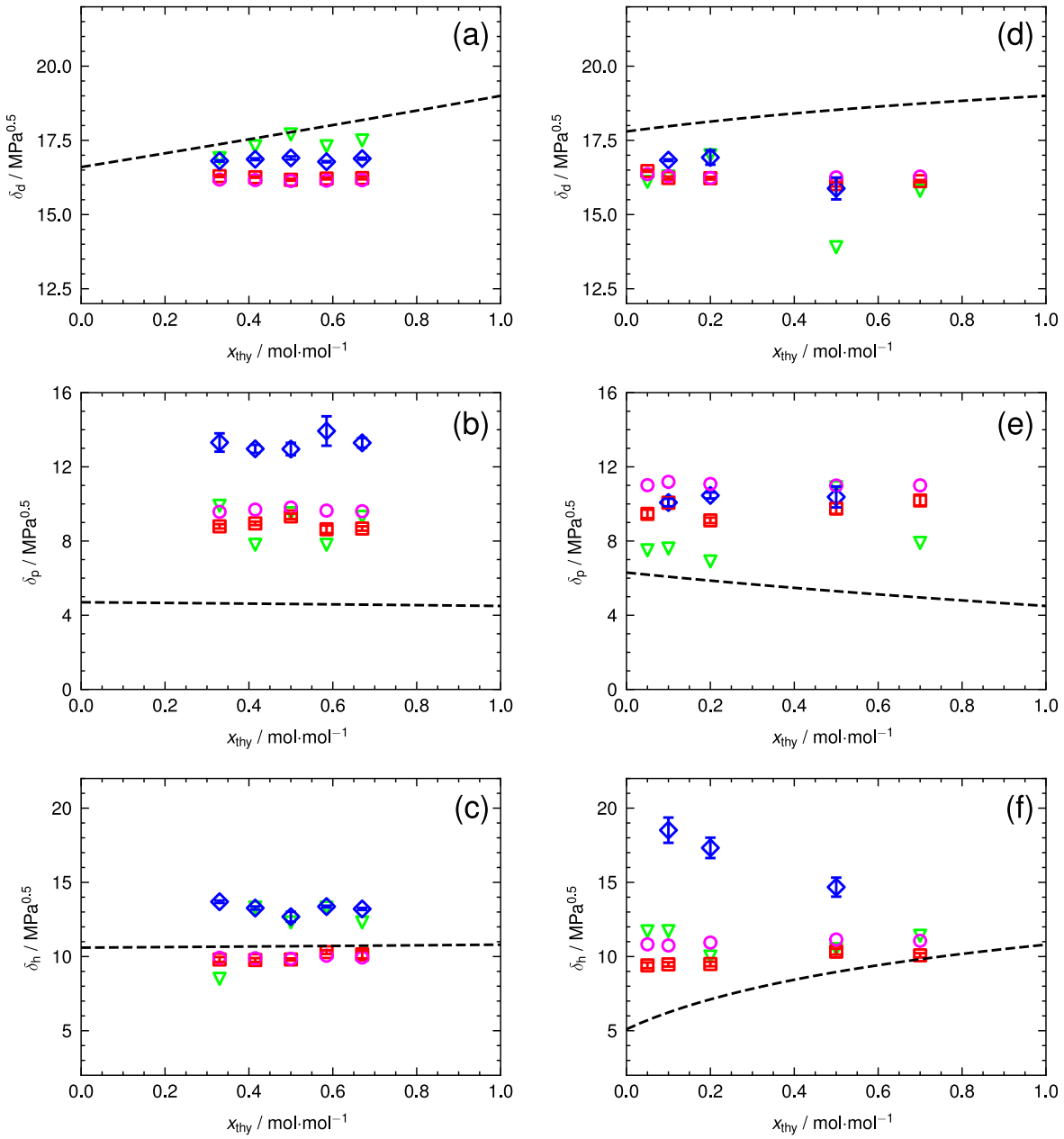


Figure 3.4.: HSP values calculated for TM (left panel) and TC (right panel), using the solubility test method HSP1 (▽), and the intrinsic viscosity based methods HSP2-S (□), HSP2-B (◇), and FSP (○), as a function of the mole fraction of thymol, $x_{thy}$, at 298.15 K. Predictions calculated using Eq. 1.7 are also included (- - -).

in the direct experimental measurements (e.g. mass or viscosity) would cause significant errors in the calculated HSP values using the HSP2-B method, as observed in the error bars of the HSP2-B method in Fig. 3.4 compared to HSP2-S. Therefore, the following discussion will focus on the HSP1, HSP2-S, and FSP methods.

It is important to remember the nature of the methods by which one tries to arrive at some

numerical value for the solubility parameters from experimental information. On the one hand, some methods estimate the cohesive energy between molecules by measuring a property directly from the system, e.g. vaporization enthalpy. On the other hand, methods like those used in this study estimate the HSP by using information regarding how the molecules of the system interact with other compounds. Although the latter vary in the level of detail in which the interactions are represented (intrinsic viscosity methods allow to distinguish how "good" a solvent is, unlike the binary classification HSP1 method), these still rely on the similarity principle, which assumes that if the DES and other compound exhibit high interactions, one could expect those to have similar HSP. Since this thermodynamic model relies on pairwise interactions, the parameters can quantify the specific interaction abilities of the molecules [28, 90, 91]. Consequently, to use the HSP theory to investigate the solvation behavior of DESs, it is necessary to determine whether the similarity principle alone accounts for the interactions between DESs and other compounds.

To this end, Fig. 3.5 shows the $\ln \gamma_i^{\infty}$ values calculated using openCOSMO-RS for 325 compounds in TM and TC at a 1:1 HBA:HBD ratio as a function of each contribution to the HSP. It should be noted that the calculation of $\ln \gamma_i^{\infty}$ using openCOSMO-RS is independent of the simplifying assumptions of Hansen theory; it merely illustrates the patterns of HSP values when sorted according to $\ln \gamma_i^{\infty}$. Fig. 3.5 shows that, in general, the interactions represented by intrinsic viscosity are qualitatively coherent with the openCOSMO-RS calculations, as seen by the position of the vertical lines with respect to the negative values of $\ln \gamma_i^{\infty}$.

Nevertheless, in some cases (e.g., Fig. 3.5.d), there is not a clear tendency, as the negative values of $\ln \gamma_i^{\infty}$ are quite scattered. The observed mismatches between the vertical lines and the $\ln \gamma_i^{\infty}$ minimum may arise due to various factors. As a simple illustration, we calculated a $\ln \gamma_i^{\infty}$-weighted average of each HSP contribution using the compounds that exhibit $\ln \gamma_i^{\infty} < -2$ for each DES. This provides an estimation of where each HSP would be positioned solely based on the $\ln \gamma_i^{\infty}$ values. Table 3.1 presents the differences between these values and those obtained with each model. The total difference, $\Delta\delta_{\text{total}}$, is also provided.

As expected, the ideal model demonstrates the largest deviation, which can be attributed principally to the underprediction of the polar contribution. This is not surprising, considering that the values are derived from a simple mole fraction average of each contribution from the pure components, neglecting the potential changes in the interaction type that may occur upon mixing. Among the other two methods, FSP exhibits the smallest deviation for both DES, with differences below 1 $\text{MPa}^{0.5}$ for each parameter. This is particularly remarkable since by only using the $[\eta]$ values of 8 solvents obtained with an approximation (Eq. 2.1), and even the visual discrimination of the HSP1 method, one can reasonably capture the interaction tendency of a much larger set of compounds.

The deviations in $\delta_{\text{d}}$ can be explained by considering that the cohesive energy of DESs and its compounds primarily originates from specific interactions, which encompass polar and hydrogen bonding forces. Furthermore, since every system experiences dispersive interactions irrespective of the nature of the molecules involved, the strength of the interactions between a DES and another compound is primarily governed by specific interactions. Hence, differences in $\delta_{\text{d}}$ between a given compound and a DES would generally not dictate the strength of the interaction. For instance, methanol ($\delta_{\text{d}}$ = 14.7 $\text{MPa}^{0.5}$, $\delta_{\text{p}}$ = 12.3 $\text{MPa}^{0.5}$, $\delta_{\text{h}}$ = 22.3 $\text{MPa}^{0.5}$) is a good solvent for benzamide [92] ($\delta_{\text{d}}$ = 21.2 $\text{MPa}^{0.5}$, $\delta_{\text{p}}$ = 14.7 $\text{MPa}^{0.5}$, $\delta_{\text{h}}$ = 11.2 $\text{MPa}^{0.5}$), even though they have a difference in $\delta_{\text{d}}$ of 6.5 $\text{MPa}^{0.5}$. However, from the methods used here, it cannot be said which one better isolates the dispersion interactions in the mixture at a molecular level. Methods with greater theoretical robustness could be suit-

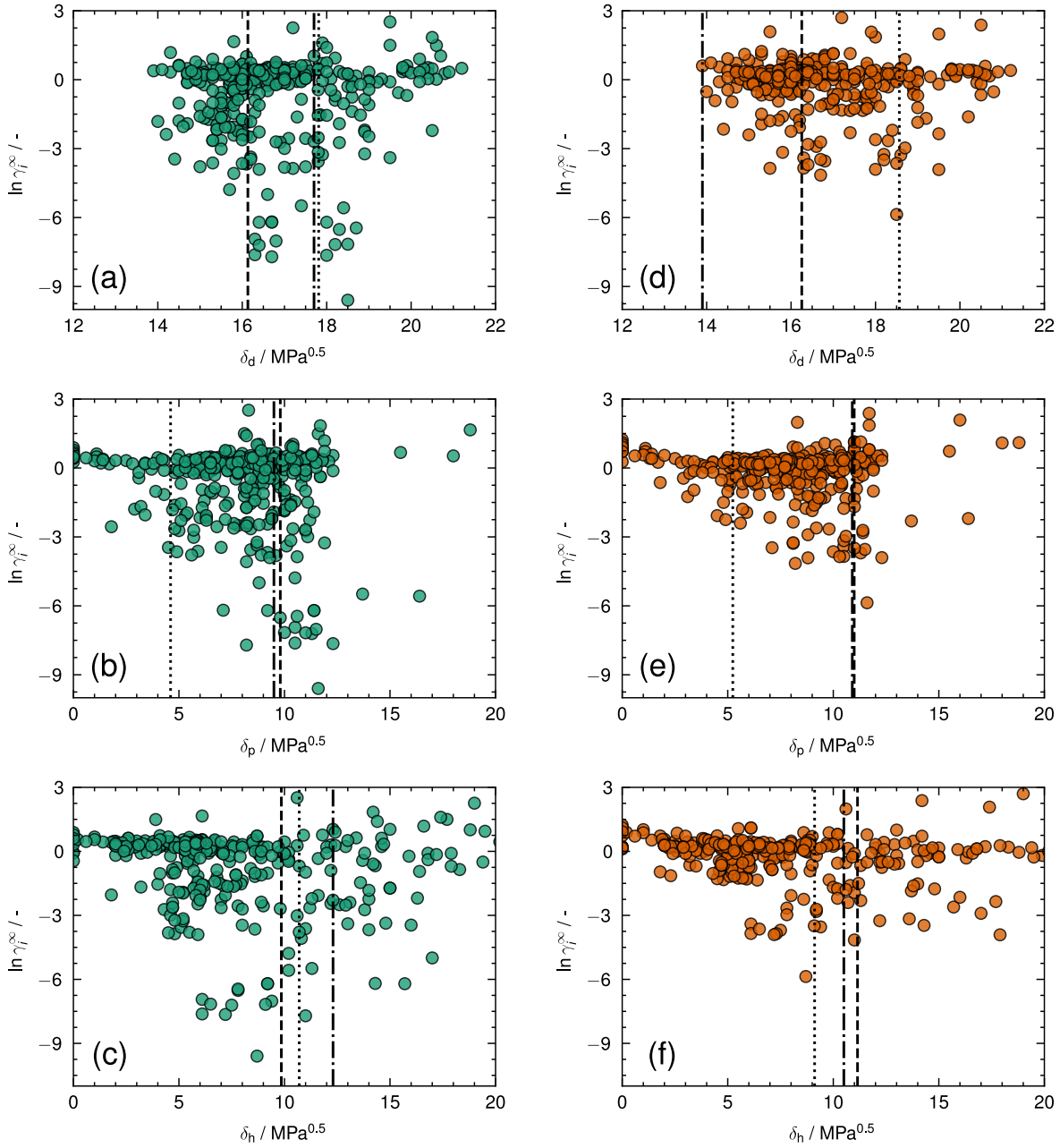


Figure 3.5.: Logarithmic activity coefficients at infinite dilution calculated using openCOSMO-RS expressed as a function of the HSP. Calculations were made for 325 solutes diluted in TM (left panel) and TC (right panel) in a 1:1 HBA:HBD molar ratio. Vertical lines correspond to the respective HSP calculated with FSP (- - -), HSP1 (-···-), and Eq. 1.7 (·····).

able for this task, such as the one recently developed by Gaudin et al. [93], which would be interesting to compare.

The deviations observed for the polar contribution can be rationalized, considering the

Table 3.1.: Differences between the $\ln \gamma_i^{\infty}$-weighted average values of each HSP contribution, and the values obtained with three of the used methods, expressed in $MPa^{0.5}$. The total difference refers to $\Delta\delta_{total} = \Delta\delta_d + \Delta\delta_p + \Delta\delta_h$.

| | TM0.5 | | | | TC0.5 | | | |
|---|---|---|---|---|---|---|---|---|
| Model | $\Delta\delta_d$ | $\Delta\delta_p$ | $\Delta\delta_h$ | $\Delta\delta_{total}$ | $\Delta\delta_d$ | $\Delta\delta_p$ | $\Delta\delta_h$ | $\Delta\delta_{total}$ |
| FSP | 0.98 | 0.43 | 0.62 | 2.03 | 1.02 | 1.15 | 0.42 | 2.60 |
| HSP1 | 0.59 | 0.73 | 3.07 | 4.39 | 3.37 | 1.06 | 0.23 | 4.67 |
| Ideal | 0.66 | 5.62 | 1.47 | 7.75 | 1.25 | 4.54 | 1.77 | 7.57 |

cumbersome empirical division of the total cohesive energy in the three contributions. It is difficult to have any degree of certainty about the interactions contributing to $\delta_p$. Even if a solvent is slightly polar regarding dipole-dipole interactions, which would allegedly translate into low $\delta_p$ values, a polar solute might induce a dipole in the solvent molecules surroundings, giving rise to induced dipole-dipole interactions. Moreover, in the case of thymol, benzene rings form quadrupoles that, although not contribute to the dipole moment of the molecule, may contribute to quadrupole-dipole interactions.

Regarding the two observations mentioned at the beginning of this section, it has to be kept in mind that the conclusions that can be drawn from Fig. 3.4 and 3.5 are limited by the methods used. As mentioned earlier the HSP values calculated from intrinsic viscosity values do not represent an inherent property of DES, but rather how these solvents interact with other substances. Thus, the estimated HSP for the DES result from weighting the HSP of each solvent by its affinity with the DES, measured by $[\eta_i]$. Accordingly, the deviations observed in Fig. 3.4 are not the deviations of inherent $\delta_d, \delta_p$ and $\delta_h$ values of each DES, but a consequence of the ability of the DES to display different polar or hydrogen bonding behavior, depending on the solute chemistry. The solvation behavior of the DES is simplified by attempting to assign a unique value to each of the HSP where higher solute-DES interactions are observed, even when this may happen in a broad range of values in the Hansen space (as observed in Fig. 3.5). Accordingly, the non-dependence of the HSP with $x_{thy}$ observed in Fig. 3.4 only indicates that the degree of affinity of each system with the different chemicals is not affected by its HBA:HBD molar ratio.

This is one of the reasons why a mixing rule such as the one mentioned in Objective 4 was not further developed. Although with expressions based on preferential solvation theory, particularly those based on the work of Bosch et al. [94], it is possible to adjust for deviations such as those shown in Fig. 3.4, such an expression would be of little use. The advantage of fitting this rule was to be able to use the vast amount of HSP reported for pure substances. However, since the calculated HSPs show no distinguishable dependence on mole fraction, fitting a function of the type $HSP_{mix} = f(HSP_{pures}, x_1)$ would result in overfitting, naturally being futile in practical terms.

Nevertheless, it must be noted that the results will most likely differ if the HSP of the systems considered here are determined using correlations that relate the HSP to bulk features of the mixture. The values here reported were obtained by "forcing" the solubility parameters to match the similarity principle, according to the experimental measurements. Another significant mention is that the HSP of the DES precursors were obtained from the handbook of Hansen [1], as it is a widely used reference. However, from the values there reported, only cy-

clohexanone has some experimental confirmation, while thymol and L-menthol come from group contribution calculations. It is possible that Eq. 1.7 could represent the experimental values of the mixture if the same methods determined the HSP of the pure compounds. The high dependence of HSP values on the method used to calculate them is one significant drawback and reason for questioning the theory. However, it is essential to remember that the extent to which any method can be said to "work" depends on the precision expected and needed for specific applications. Thus, the following section discusses the applicability of the calculated HSP for prediction purposes.

### 3.3.2. Solubility estimations of solids in DES

The evaluation of the predictive capabilities for the HSP of DES follows the same structure as in Section 3.2. Table 3.2 shows the experimental solubility of quercetin and curcumin in TM at different HBA:HBD molar ratios, along with the RMSLD values for each model. Compared to the other models, the best performance is observed for openCOSMO-RS (RMSLD = 0.27), which is close to what has been reported in other studies [88, 95, 96], within ranges between 0.2 and 0.5 log units. As expected, the FH-HSP model underpredicts the solubility in the four cases (RMSLD = 0.86). Moreover, using the ideal HSP calculated with Eq. 1.7 gives further underpredictions, scoring the highest error (RMSLD = 1.13). However, it is impossible to obtain a representative metric about the performance of each model by using only these datapoints. Unfortunately, experimental data that includes both solubility in the studied DES and the melting properties of the solutes is scarce. For this reason, the three models were compared by calculating the solubility of 21 solid solutes (indicated in the Excel file in the Supporting Information) in each of the thymol mole fractions studied, resulting in 210 solute-DES pairs. Since openCOSMO-RS showed better performance in the cases discussed above, its predictions were used as the reference value for comparison purposes. The predictions resulted in differences of 0.76, 0.70, and 0.71 log units for FH-HSP using Eq. 1.7, FH-HSP using the FSP values, and PC-SAFT, respectively, with respect to openCOSMO-RS.

Additionally, the predictions of each model are depicted as violin plots in Fig. 3.6. Here, the width of each histogram along the y-axis represents the density distribution of the number of solute-DES pairs predicted at that mole fraction range. It is observed that the FH-HSP and PC-SAFT give similar predictions, with no significant differences between the distributions of both DES. Additionally, in both models, most of the values are located at low mole fractions. However, openCOSMO-RS tend to estimate larger solubility values for more solutes in both DES, as seen by the width of the distribution above 0.25 $\text{mol} \cdot \text{mol}^{-1}$. Moreover, it indicates that TC gives higher solubility for more solutes near 0.4 $\text{mol} \cdot \text{mol}^{-1}$.

Although similar performances for FH-HSP and PC-SAFT are observed, it should be noted that the ability of PC-SAFT to accurately predict mixture phase equilibria for complex systems of unlike molecules without using any binary interaction parameters fitted to experimental data is generally limited. Of course, this purely predictive capacity can be improved by using interaction parameters, which is also one of the advantages of PC-SAFT.

Additionally, FH-HSP predictions are limited to the temperature at which the HSP were calculated, while PC-SAFT and openCOSMO-RS can integrate this dependence. Nevertheless, it is interesting to see that a simple model such as FH-HSP provides reasonable estimations for DES when compared to the purely predictive parametrization of PC-SAFT. For future work, it would be valuable to obtain experimental confirmation on the solid solubility in the type of DES studied here, particularly for solutes that exhibit high predicted solubilities

in all the models.

For the qualitative evaluation of the HSP, the screening parameters RED and $\ln \gamma_i^{\infty}$ were calculated for 26 solid solutes (refer to the Excel file in the Supporting Information), each in TM and TC at the five thymol concentrations. Fig. 3.7 shows the matches and mismatches between both approaches. A comparison is made between the RED values computed using the values from the FSP method (Fig. 3.7a) and the ideal HSP from Eq. 1.7 (Fig. 3.7b). Interestingly, the number of matches (quadrants I and III) is similar in both cases, with 70.4% and 68.5% for Fig. 3.7a and 3.7b, respectively. Regarding the mismatches, the FSP values perform slightly better since quadrant IV contains 6.9% of the pairs, compared to 10.4% when using the ideal HSP. The latter introduces some extra false negatives in quadrant IV, which are worse errors as these leave out potentially suitable candidates. For example, openCOSMO-RS shows TC is a great candidate for dissolving quercetin, corresponding to the most negative $\ln \gamma_i^{\infty}$ values in the III quadrants. However, only the FSP values are accordant to this, as seen by RED $< 1$ values. This may be explained by the higher polar contribution calculated for TC when using the FSP, and as quercetin has a high polar contribution ($\delta_p = 16.85$ MPa$^{0.5}$), the prediction improves. Moreover, the ideal HSP displaces several points to the left, indicating RED predicting stronger interactions when openCOSMO-RS suggests only slight ones.

The results indicate that the HSP are unsuitable for accurately predicting DES solubility if a high or intermediate level of numerical accuracy is needed. However, the HSP theory can still provide a valuable tool for screening processes in DES applications. Specifically, it can broadly capture the trend in DES-solute affinities compared to the more accurate $\ln \gamma_i^{\infty}$ values. This makes the HSP approach advantageous during the initial screening phase, when many candidates must be evaluated. Using more refined techniques may demand high computational costs. Thus, the HSP method can provide a cost-effective and time-saving alternative.

Table 3.2.: Experimental and calculated solubilities of quercetin and curcumin in TM. FH-HSP predictions using the HSP from the FSP method and the ideal mixing expression (Eq. 1.7) are included. RMSLD with respect to the experimental value is also shown.

| | | Mole fraction solubility | | | | |
|---|---|---|---|---|---|---|
| Solute | HBA:HBD mole ratio | Experimental | FH-HSP (Eq. 1.7) | FH-HSP (FSP) | openCOSMO-RS | PC-SAFT |
| Quercetin | 1:2 | $1.27 \cdot 10^{-3}$ [41] | $5.40 \cdot 10^{-5}$ | $1.37 \cdot 10^{-4}$ | $4.07 \cdot 10^{-3}$ | $2.55 \cdot 10^{-4}$ |
| | 1:1 | $5.93 \cdot 10^{-4}$ [41] | $5.40 \cdot 10^{-5}$ | $1.42 \cdot 10^{-4}$ | $9.23 \cdot 10^{-4}$ | $2.56 \cdot 10^{-4}$ |
| | 2:1 | $3.32 \cdot 10^{-4}$ [41] | $5.20 \cdot 10^{-5}$ | $1.39 \cdot 10^{-4}$ | $2.79 \cdot 10^{-4}$ | $2.56 \cdot 10^{-4}$ |
| Curcumin | 5:8 | $2.74 \cdot 10^{-2}$ [97] | $1.70 \cdot 10^{-3}$ | $1.64 \cdot 10^{-3}$ | $2.65 \cdot 10^{-2}$ | $5.65 \cdot 10^{-4}$ |
| | | RMSLD | 1.13 | 0.86 | 0.27 | 0.93 |

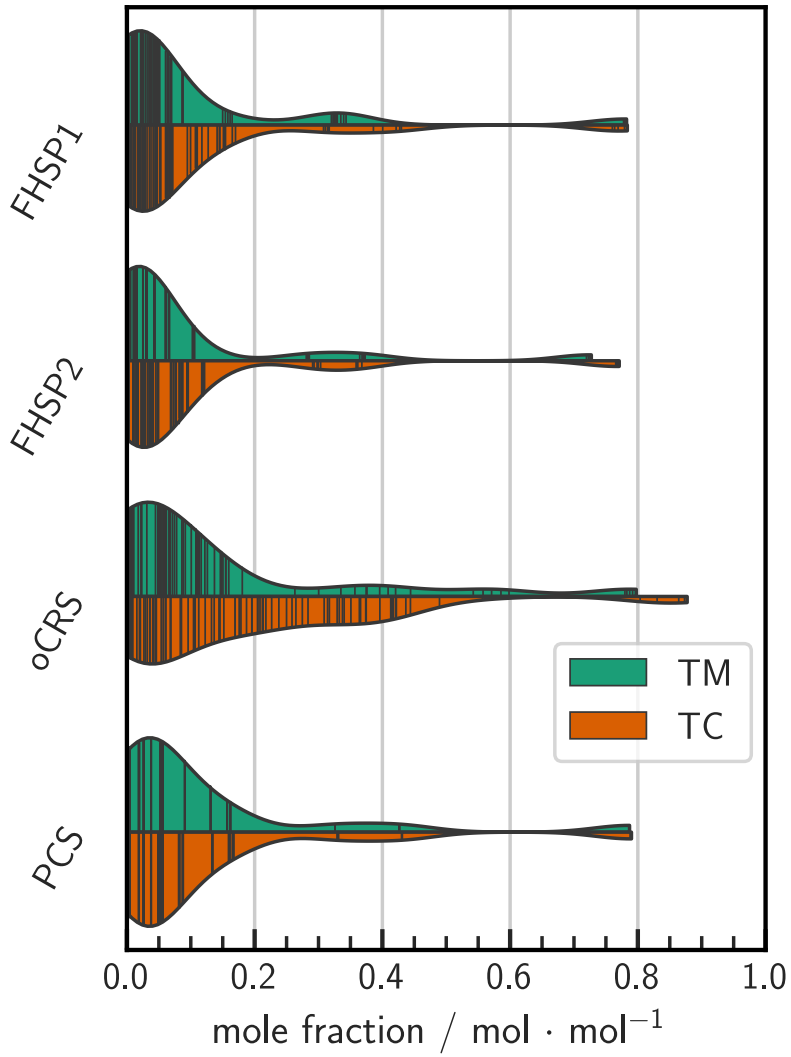


Figure 3.6.: Violin plots representations of solubility predictions for solid solutes in TM and TC. The models are: FH-HSP using the HSP from Eq. 1.7 (FHSP1), FH-HSP using the FSP method (FHSP2), openCOSMO-RS (oCRS), and PC-SAFT (PCS). The violin plot shows kernel density trace or smoothed histograms to describe the data distribution pattern. The width of the violin at any point represents the density of data points at that particular mole fraction. Black lines inside the curves represent the datapoints.

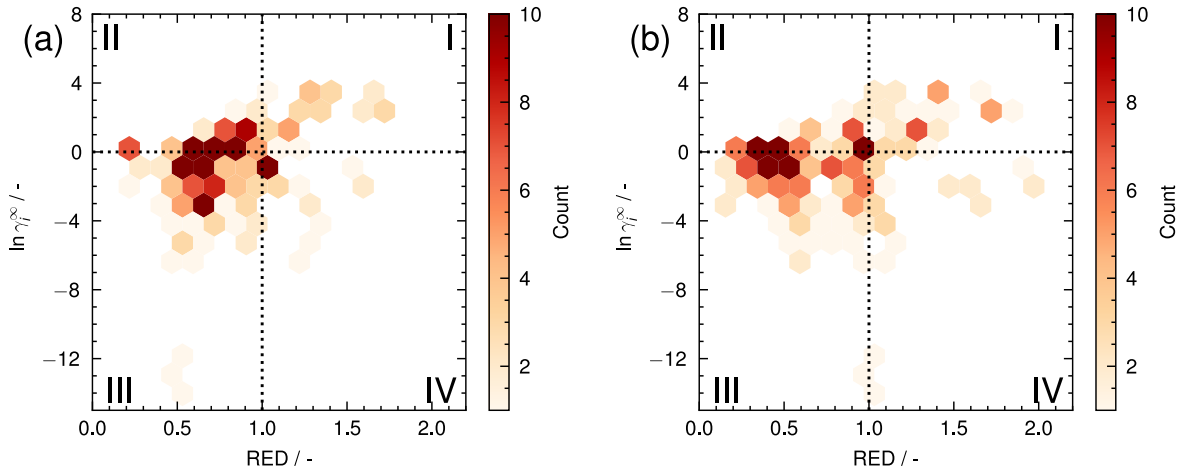


Figure 3.7.: Hexbin plot showing the relationship between predicted $\ln \gamma_i^\infty$ using openCOSMO-RS and the RED parameter between a pure solid solute $i$ and a DES at 298.15 K. The color intensity represents the number of points in each hexagon. RED was calculated using the HSP obtained with (a) the FSP method and (b) ideal values from Eq. 1.7. Both subfigures are divided into four quadrants, representing the matches (I and III) and mismatches (II and IV) between both screening parameters

# 4. Conclusions

This study aimed to assess the efficacy of using HSP to predict solid solubility in DES and its screening capabilities. Although HSP theory is commonly used in screening processes, its applicability to systems with strong specific molecular interactions is limited. Two DES (TM and TC) and their respective precursors were investigated to test the HSP model. The predictions of the FH-HSP model were compared with openCOSMO-RS and PC-SAFT models using solubility calculations. These were contrasted with experimental data reported in the literature. The RED parameter of the HSP was used to evaluate its screening capabilities against $\ln \gamma_i^{\infty}$ values calculated with openCOSMO-RS.

The obtained HSP values of each DES deviated from the ideal mixing rules and did not show a dependence on the thymol mole fraction. The calculated HSP captured the interactions between a large set of chemicals of different natures and the studied DES, as measured by the calculated $\ln \gamma_i^{\infty}$. Among the methods employed, the FSP approach exhibited the best performance.

The FH-HSP model performed reasonably well in predicting the solubility of thymol and L-menthol in organic solvents, with deviations of 0.12 and 0.11 log units, respectively. Additionally, for these same substances, the RMSLD values were lower for openCOSMO-RS (0.02 for thymol and 0.04 for L-menthol) and similar for PC-SAFT (0.11 log units for both). In contrast, all three models showed more significant deviations in predicting the solubility of solid compounds in cyclohexanone. Specifically, FH-HSP, openCOSMO-RS, and PC-SAFT had RMSLD values of 0.46, 0.63, and 0.55 log units, respectively.

Regarding screening assessment, out of 2204 solute-solvent pairs evaluated, the RED parameter showed a 66% match rate compared to $\ln \gamma_i^{\infty}$, with 12% false negatives.

For solubility predictions in DES compared to available experimental data, all models showed higher RMSLD values, with FH-HSP, openCOSMO-RS, and PC-SAFT yielding 0.86, 0.27, and 0.93 log units, respectively. Using FH-HSP with HSP obtained from an ideal mixing rule of the parameters of pure compounds resulted in a deviation of 1.13 log units. The screening assessment of the studied DES revealed a 70% match rate between the RED parameter and $\ln \gamma_i^{\infty}$, with 6.9% false negatives. Using HSP obtained from the ideal mixing rule resulted in similar scores, with 68.5% match rate and 10.4% false negatives.

The results of this work indicate that the HSP are not recommended for solubility calculations in DES if high accuracy is required. However, it can be a useful tool for differentiating between "good" and "bad" solvents and for guiding the selection of potential DES-solute pairs. This makes it a valuable aid in screening processes, especially during the initial stages when many candidates must be evaluated. By using HSP theory to identify promising solvents, computational resources can be focused on a smaller set of compounds using more refined methods.

## 4.1. Assessment of the hypotheses

Based on the results obtained from this project, the following answers can be given for the hypotheses proposed at the beginning:

1. *Hansen solubility parameters allow for the calculation of the solubility of solid solutes in deep eutectic solvents.* No. The solubility calculated for solid solutes in the studied DES, using the FH-HSP model, gives results with important deviations. This was evidenced when comparing the predictions with experimental data for quercetin and curcumin in TM. Moreover, large deviations were observed for other solutes when compared to openCOSMO-RS, which was the model that performed the best in most cases. Hence, this model is not recommended if a high level of accuracy is needed. It must be mentioned that these calculations assume that the precipitation of the solid solute occurs as a pure compound. Therefore, the formation of co-crystals between the solute and the components of the DES is not considered, which may contribute to the errors of all the models. However, the obtained HSP were found to be useful for screening tasks using the RED parameter.

2. *Intrinsic viscosity allows the determination of Hansen solubility parameters values for deep eutectic solvents, which can be used to predict the solubility of these systems with solid solutes.* Yes. By calculating the intrinsic viscosity of the studied DES, it was possible to calculate HSP values for these solvents. The obtained HSP was better than the ones obtained from Eq. 1.7 for capturing the interactions between the DES and other substances. This was shown by the calculated $\ln \gamma_i^{\infty}$ using openCOSMO-RS (Fig. 3.5). Although using the HSP from intrinsic viscosity calculations for estimating the solubility of solid solutes in the DES resulted in smaller deviations than when using Eq. 1.7, is still not suited for quantitatively accurate solubility predictions.

3. *The Hansen solubility parameters of deep eutectic solvents deviate from linear behavior with respect to composition.* Yes. However, this was evaluated by using HSP obtained from information regarding the affinity of the DES with other compounds, along with the HSP of those compounds. Therefore, a better affirmation would be that “the HSP of a binary DES that best represents its interactions with other compounds deviates from a linear behavior”. Nevertheless, one must be aware that the HSP for any compound hardly have “true” reference values, since its origin is an empirical, although convenient, division in additive contributions to the total molar cohesive energy. This brings up the question of how would one proceed to define "true" or rigorous HSP values for a mixture, since this should be established in order to talk about deviations from an ideal thermodynamic behavior. For instance, it is quite intuitive to see that the Hildebrand parameter of a mixture is a well-defined quantity, since in principle it would be approximately given by the heat of vaporization of the system at that composition minus $RT$. However, it would be hard to distinguish what portion of that energy is due to dispersive forces, polar interactions, or hydrogen bonding interactions. In this sense, Gaudin et al. [93] recently described an alternative for calculating the dispersive HSP contribution, $\delta_{\mathrm{d}}$, by introducing the concept of COSMOmorph (the molecule is depicted as a COSMO cavity with all surface charge densities and dielectric energy equal to zero), addressing the splitting in a more rigorous way. However, a similar treatment has not been developed for the polar and hydrogen bonding contributions. Despite the above

mentioned, in terms of practical application, it is helpful to know that if one estimates the HSP of a DES by using Eq. 1.7, less accuracy should be expected in terms of affinity predictions than if one calculates them from experimental measurements, such as intrinsic viscosity.

## 4.2. Outlook

The motivation for this investigation was embedded in the context of solvent screening for polymer dissolution using alternative solvents. As DES were the chosen solvents, this led to the more specific question of whether HSP could be used for these solvents in the first place. The results of this study helped to discern the capabilities of this approach when applied to DES.

Regarding the solubility parameters in general, it is the author's opinion that efforts should not be concentrated on developing more methods to predict HSPs aimed at reducing the error, as long as these errors are calculated using as reference the values reported in the Hansen manual. This is in no way meant to diminish the importance of the contribution of this database. Rather, it is to highlight the bottleneck that the HSP theory inherently has. In this context, undoubtedly the most important progress that has been made in exploiting the concept of solubility parameters is the development made by Panayiotou [98]. The extension of HSPs to partial solubility parameters and their integration into an equation of state framework has been shown to be successful in predicting thermodynamic properties [99–101]. However, it has failed to take off in the scientific community. In this context, an interesting effort would be to implement the framework developed by Panayiotou in a freely available library, written in a widely used language, such as Python or Julia.

Regarding the continuation of the work conducted in this investigation, future work at the group should focus on developing a systematic workflow for solvent screening for polymers of interest. Such a methodology would benefit from integrating the HSP approach in the first stages, as it would reduce the computational cost by filtering easy-to-distinguish bad solvents. For more rigorous calculations, openCOSMO-RS appears as a great alternative. As an open-access tool, it would be of interest to investigate, for example, the optimal way of representing polymers for the COSMO-RS calculations, in terms of chain length, terminal groups, and combinatorial contribution of the activity coefficients. As an open-source implementation, openCOSMO-RS invites to try various interesting tasks. For instance, optimization of the element-scaling descriptors to evaluate the potential improvement on the predictions by using available experimental data, or the addition of equilibrium routines into the library.

# List of Acronyms

| | |
|---|---|
| **COSMO-RS** | **CO**nductor-like **S**creening **MO**del for **R**eal **S**olvents |
| **DES** | **D**eep **E**utectic **S**olvent |
| **FH-HSP** | **F**lory-**H**uggins **H**ansen **S**olubility **P**arameters model |
| **FSP** | **F**unctional **S**olubility **P**arameters |
| **HBA** | **H**ydrogen **B**ond **A**cceptor |
| **HBD** | **H**ydrogen **B**ond **D**onor |
| **HSP** | **H**ansen **S**olubility **P**arameters |
| **HSP1** | Method 1 for calculating HSP |
| **HSP2-B** | Method 2 for calculating HSP, using Bustamante equation |
| **HSP2-S** | Method 2 for calculating HSP, using Segarceanu equation |
| **PC-SAFT** | **P**erturbed-**C**hain **S**tatistical **A**ssociating **F**luid **T**heory |
| **RMSLD** | **R**oot-**M**ean-**S**quared **L**ogarithmic **D**eviation |
| **TC** | **T**hymol + **C**yclohexanone |
| **TM** | **T**hymol + L-**M**enthol |

# Bibliography


[1] Charles M. Hansen. *Hansen Solubility Parameters: A User's Handbook, Second Edition*. CRC Press, Boca Raton, 2007. ISBN 9780849372483. URL https://www.routledge.com/Hansen-Solubility-Parameters-A-Users-Handbook-Second-Edition/Hansen/p/book/9780849372483.

[2] Mónia A. R. Martins, Simão P. Pinho, and João A. P. Coutinho. Insights into the Nature of Eutectic and Deep Eutectic Mixtures. *Journal of Solution Chemistry*, 48(7): 962–982, aug 2018. doi: 10.1007/s10953-018-0793-1. URL https://doi.org/10.1007%2Fs10953-018-0793-1.

[3] Dinis O. Abranches, Liliana P. Silva, Mónia A. R. Martins, Simão P. Pinho, and João A. P. Coutinho. Understanding the Formation of Deep Eutectic Solvents: Betaine as a Universal Hydrogen Bond Acceptor. *ChemSusChem*, 13(18):4916–4921, aug 2020. doi: 10.1002/cssc.202001331. URL https://doi.org/10.1002%2Fcssc.202001331.

[4] Adriaan van den Bruinhorst and Margarida Costa Gomes. Is there depth to eutectic solvents? *Current Opinion in Green and Sustainable Chemistry*, 37:100659, oct 2022. doi: 10.1016/j.cogsc.2022.100659. URL https://doi.org/10.1016%2Fj.cogsc.2022.100659.

[5] Maximilian Neubauer, Thomas Wallek, and Susanne Lux. Deep eutectic solvents as entrainers in extractive distillation – A review. *Chemical Engineering Research and Design*, 184:402–418, aug 2022. doi: 10.1016/j.cherd.2022.06.019. URL https://doi.org/10.1016%2Fj.cherd.2022.06.019.

[6] Kristina Radošević, Marina Cvjetko Bubalo, Višnje Gaurina Srček, Dijana Grgas, Tibela Landeka Dragičević, and Ivana Radojčić Redovniković. Evaluation of toxicity and biodegradability of choline chloride based deep eutectic solvents. *Ecotoxicology and Environmental Safety*, 112:46–53, feb 2015. doi: 10.1016/j.ecoenv.2014.09.034. URL https://doi.org/10.1016%2Fj.ecoenv.2014.09.034.

[7] Karzan A. Omar and Rahmat Sadeghi. Physicochemical properties of deep eutectic solvents: A review. *Journal of Molecular Liquids*, 360:119524, aug 2022. doi: 10.1016/j.molliq.2022.119524. URL https://doi.org/10.1016%2Fj.molliq.2022.119524.

[8] Sudhir Ravula, Nathaniel E. Larm, Mohammad A. Mottaleb, Mark P. Heitz, and Gary A. Baker. Vapor Pressure Mapping of Ionic Liquids and Low-Volatility Fluids Using Graded Isothermal Thermogravimetric Analysis. *ChemEngineering*, 3(2):42, apr 2019. doi: 10.3390/chemengineering3020042. URL https://doi.org/10.3390%2Fchemengineering3020042.

[9] Qing Wen, Jing-Xin Chen, Yu-Lin Tang, Juan Wang, and Zhen Yang. Assessing the toxicity and biodegradability of deep eutectic solvents. *Chemosphere*, 132:63–69, aug

2015. doi: 10.1016/j.chemosphere.2015.02.061. URL https://doi.org/10.1016%2Fj.chemosphere.2015.02.061.

[10] Maan Hayyan, Yves Paul Mbous, Chung Yeng Looi, Won Fen Wong, Adeeb Hayyan, Zulhaziman Salleh, and Ozair Mohd-Ali. Natural deep eutectic solvents: cytotoxic profile. *SpringerPlus*, 5(1), jun 2016. doi: 10.1186/s40064-016-2575-9. URL https://doi.org/10.1186%2Fs40064-016-2575-9.

[11] Javier Torregrosa-Crespo, Xavier Marset, Gabriela Guillena, Diego J. Ramón, and Rosa María Martínez-Espinosa. New guidelines for testing "Deep eutectic solvents" toxicity and their effects on the environment and living beings. *Science of The Total Environment*, 704:135382, feb 2020. doi: 10.1016/j.scitotenv.2019.135382. URL https://doi.org/10.1016%2Fj.scitotenv.2019.135382.

[12] Stefano Nejrotti, Achille Antenucci, Carlotta Pontremoli, Lorenzo Gontrani, Nadia Barbero, Marilena Carbone, and Matteo Bonomo. Critical Assessment of the Sustainability of Deep Eutectic Solvents: A Case Study on Six Choline Chloride-Based Mixtures. *ACS Omega*, 7(51):47449–47461, dec 2022. doi: 10.1021/acsomega.2c06140. URL https://doi.org/10.1021%2Facsomega.2c06140.

[13] Matilde Vieira Sanches, Rosa Freitas, Matteo Oliva, Angelica Mero, Lucia De Marchi, Alessia Cuccaro, Giorgia Fumagalli, Andrea Mezzetta, Greta Colombo Dugoni, Monica Ferro, Andrea Mele, Lorenzo Guazzelli, and Carlo Pretti. Are natural deep eutectic solvents always a sustainable option? A bioassay-based study. *Environmental Science and Pollution Research*, 30(7):17268–17279, oct 2022. doi: 10.1007/s11356-022-23362-5. URL https://doi.org/10.1007%2Fs11356-022-23362-5.

[14] Hemayat Shekaari, Mohammed Taghi Zafarani-Moattar, Masumeh Mokhtarpour, and Saeid Faraji. Deep eutectic solvents for antiepileptic drug phenytoin solubilization: thermodynamic study. *Scientific Reports*, 11(1), dec 2021. doi: 10.1038/s41598-021-03212-z. URL https://doi.org/10.1038%2Fs41598-021-03212-z.

[15] Yue Wu, Wen Li, Jessica Vovers, Hiep Thuan Lu, Geoffrey W. Stevens, and Kathryn A. Mumford. Investigation of green solvents for the extraction of phenol and natural alkaloids: Solvent and extractant selection. *Chemical Engineering Journal*, 442:136054, aug 2022. doi: 10.1016/j.cej.2022.136054. URL https://doi.org/10.1016%2Fj.cej.2022.136054.

[16] Mark D. Lawley, David Boon, Lisa Y. Stein, and Dominic Sauvageau. Switchable Solvents for the Reversible Dissolution of Poly(3-hydroxybutyrate). *ACS Sustainable Chemistry & Engineering*, 10(8):2602–2608, feb 2022. doi: 10.1021/acssuschemeng.1c06377. URL https://doi.org/10.1021%2Facssuschemeng.1c06377.

[17] Joel Henry Hildebrand and Robert Lane Scott. *The Solubility of Nonelectrolytes*. Reinhold Publishing Corporation, 1950.

[18] Emmerich Wilhelm and Trevor Letcher, editors. *Enthalpy and Internal Energy*. Royal Society of Chemistry, Cambridge, England, September 2017. ISBN 978-1-78801-021-4. doi: https://doi.org/10.1039/9781788010214.

[19] Allan F M Barton. *CRC Handbook of Solubility Parameters and Other Cohesion Parameters, Second Edition*. CRC Press, Boca Raton, FL, 2 edition, October 1991.

[20] Manuel Díaz de los Ríos and Rubén Murcia Belmonte. Extending Microsoft excel and Hansen solubility parameters relationship to double Hansen's sphere calculation. *SN Applied Sciences*, 4(6), may 2022. doi: 10.1007/s42452-022-04959-4. URL https://doi.org/10.1007%2Fs42452-022-04959-4.

[21] D W Van Krevelen and Klaas Te Nijenhuis. *Properties of Polymers*. Elsevier Science & Technology, 4 edition, May 2014.

[22] Didier Mathieu. Pencil and Paper Estimation of Hansen Solubility Parameters. *ACS Omega*, 3(12):17049–17056, dec 2018. doi: 10.1021/acsomega.8b02601. URL https://doi.org/10.1021%2Facsomega.8b02601.

[23] Y. Lan, M. G. Corradini, R. G. Weiss, S. R. Raghavan, and M. A. Rogers. To gel or not to gel: correlating molecular gelation with solvent parameters. *Chemical Society Reviews*, 44(17):6035–6058, 2015. doi: 10.1039/c5cs00136f. URL https://doi.org/10.1039%2Fc5cs00136f.

[24] Bshaer M. Jameel, An Huynh, Aastha Chadha, Sujata Pandey, Jacalyn Duncan, Mark Chandler, and Gabriella Baki. Computer-based formulation design and optimization using Hansen solubility parameters to enhance the delivery of ibuprofen through the skin. *International Journal of Pharmaceutics*, 569:118549, oct 2019. doi: 10.1016/j.ijpharm.2019.118549. URL https://doi.org/10.1016%2Fj.ijpharm.2019.118549.

[25] Jinwen Qin, Xin Wang, Qiwang Jiang, and Minhua Cao. Optimizing Dispersion, Exfoliation, Synthesis, and Device Fabrication of Inorganic Nanomaterials Using Hansen Solubility Parameters. *ChemPhysChem*, 20(9):1069–1097, apr 2019. doi: 10.1002/cphc.201900110. URL https://doi.org/10.1002%2Fcphc.201900110.

[26] Ziyuan Zhou, Lei Li, Xiaoya Liu, Haoyong Lei, Wanjie Wang, Yanyu Yang, Jianfeng Wang, and Yanxia Cao. An efficient water-assisted liquid exfoliation of layered MXene (Ti3C2Tx) by rationally matching Hansen solubility parameter and surface tension. *Journal of Molecular Liquids*, 324:115116, feb 2021. doi: 10.1016/j.molliq.2020.115116. URL https://doi.org/10.1016%2Fj.molliq.2020.115116.

[27] A. F. M. Barton. Applications of solubility parameters and other cohesion parameters in polymer science and technology. *Pure and Applied Chemistry*, 57(7):905–912, jan 1985. doi: 10.1351/pac198557070905. URL https://doi.org/10.1351%2Fpac198557070905.

[28] Costas Panayiotou. Redefining solubility parameters: the partial solvation parameters. *Physical Chemistry Chemical Physics*, 14(11):3882, 2012. doi: 10.1039/c2cp23966c. URL https://doi.org/10.1039%2Fc2cp23966c.

[29] Dimitra Lazidou, Spyros Mastrogeorgopoulos, and Costas Panayiotou. Thermodynamic characterization of ionic liquids. *Journal of Molecular Liquids*, 277:10–21, mar 2019. doi: 10.1016/j.molliq.2018.12.023. URL https://doi.org/10.1016%2Fj.molliq.2018.12.023.

[30] Costas Panayiotou and Vassily Hatzimanikatis. The solubility parameters of carbon dioxide and ionic liquids: Are they an enigma? *Fluid Phase Equilibria*, 527:112828, jan 2021. doi: 10.1016/j.fluid.2020.112828. URL https://doi.org/10.1016%2Fj.fluid.2020.112828.

[31] Hemayat Shekaari, Mohammed Taghi Zafarani-Moattar, and Behrouz Mohammadi. Effective extraction of benzene and thiophene by novel deep eutectic solvents from hexane / aromatic mixture at different temperatures. *Fluid Phase Equilibria*, 484:38–52, apr 2019. doi: 10.1016/j.fluid.2018.11.025. URL https://doi.org/10.1016%2Fj.fluid.2018.11.025.

[32] Yameng Wan, Haixia He, Zibo Huang, Pengshuai Zhang, Jiao Sha, Tao Li, and Baozeng Ren. Solubility, thermodynamic modeling and Hansen solubility parameter of 5-norbornene-2,3-dicarboximide in three binary solvents (methanol, ethanol, ethyl acetate + DMF) from 278.15 K to 323.15 K. *Journal of Molecular Liquids*, 300:112097, feb 2020. doi: 10.1016/j.molliq.2019.112097. URL https://doi.org/10.1016%2Fj.molliq.2019.112097.

[33] Masumeh Mokhtarpour, Hemayat Shekaari, Mohammed Taghi Zafarani-Moattar, and Salva Golgoun. Solubility and solvation behavior of some drugs in choline based deep eutectic solvents at different temperatures. *Journal of Molecular Liquids*, 297:111799, jan 2020. doi: 10.1016/j.molliq.2019.111799. URL https://doi.org/10.1016%2Fj.molliq.2019.111799.

[34] Laura J. B. M. Kollau, Remco Tuinier, Job Verhaak, Jaap den Doelder, Ivo A. W. Filot, and Mark Vis. Design of Nonideal Eutectic Mixtures Based on Correlations with Molecular Properties. *The Journal of Physical Chemistry B*, 124(25):5209–5219, jun 2020. doi: 10.1021/acs.jpcb.0c01680. URL https://doi.org/10.1021%2Facs.jpcb.0c01680.

[35] Renren Sun, Haixia He, Yameng Wan, Lei Yuan, Liyuan Li, Jiao Sha, Gaoliang Jiang, Yu Li, Tao Li, and Baozeng Ren. Equilibrium solubility of kojic acid in four binary solvents: Determination, model evaluation, Hansen solubility parameter, thermodynamic properties and quantum chemical calculations. *Journal of Molecular Liquids*, 325:114796, mar 2021. doi: 10.1016/j.molliq.2020.114796. URL https://doi.org/10.1016%2Fj.molliq.2020.114796.

[36] Huanxin Li, Yingnan Xie, Yan Xue, peizhi Zhu, and Hongkun Zhao. Comprehensive insight into solubility, dissolution properties and solvation behaviour of dapsone in co-solvent solutions. *Journal of Molecular Liquids*, 341:117403, nov 2021. doi: 10.1016/j.molliq.2021.117403. URL https://doi.org/10.1016%2Fj.molliq.2021.117403.

[37] Hemayat Shekaari, Mohammed Taghi Zafarani-Moattar, and Masumeh Mokhtarpour. Effective ultrasonic-assisted extraction and solubilization of curcuminoids from turmeric by using natural deep eutectic solvents and imidazolium-based ionic liquids. *Journal of Molecular Liquids*, 360:119351, aug 2022. doi: 10.1016/j.molliq.2022.119351. URL https://doi.org/10.1016%2Fj.molliq.2022.119351.

[38] Mood Mohan, Kaixuan Huang, Venkataramana R. Pidatala, Blake A. Simmons, Seema Singh, Kenneth L. Sale, and John M. Gladden. Prediction of solubility parameters of

lignin and ionic liquids using multi-resolution simulation approaches. *Green Chemistry*, 24(3):1165–1176, 2022. doi: 10.1039/d1gc03798f. URL https://doi.org/10.1039%2Fd1gc03798f.

[39] Yoshihiro Takebayashi, Kiwamu Sue, Takeshi Furuya, and Satoshi Yoda. Solubilities of Organic Semiconductors and Nonsteroidal Anti-inflammatory Drugs in Pure and Mixed Organic Solvents: Measurement and Modeling with Hansen Solubility Parameter. *Journal of Chemical & Engineering Data*, 63(10):3889–3901, sep 2018. doi: 10.1021/acs.jced.8b00536. URL https://doi.org/10.1021%2Facs.jced.8b00536.

[40] Joseph R. Vella and Bennett D. Marshall. Mixture Solubility Parameters from Experimental Data and Perturbed-Chain Statistical Associating Fluid Theory. *Journal of Chemical & Engineering Data*, 65(12):5801–5808, sep 2020. doi: 10.1021/acs.jced.0c00706. URL https://doi.org/10.1021%2Facs.jced.0c00706.

[41] Fernando Bergua, Miguel Castro, Carlos Lafuente, and Manuela Artal. Thymol+l-menthol eutectic mixtures: Thermophysical properties and possible applications as decontaminants. *Journal of Molecular Liquids*, 368:120789, dec 2022. doi: 10.1016/j.molliq.2022.120789. URL https://doi.org/10.1016/%2Fj.molliq.2022.120789.

[42] Andreas Klamt. *COSMO-RS: From Quantum Chemistry to Fluid Phase Thermodynamics and Drug Design*. Elsevier Science & Technology, May 2014.

[43] Andreas Klamt. The COSMO and COSMO-RS solvation models. *Wiley Interdisciplinary Reviews: Computational Molecular Science*, 8(1), 2018. ISSN 1759-0876. doi: 10.1002/wcms.1338.

[44] José Pedro Wojeicchowski, Ana M. Ferreira, Dinis O. Abranches, Marcos R. Mafra, and João A. P. Coutinho. Using COSMO-RS in the Design of Deep Eutectic Solvents for the Extraction of Antioxidants from Rosemary. *ACS Sustainable Chemistry & Engineering*, 8(32):12132–12141, 2020. ISSN 2168-0485. doi: 10.1021/acssuschemeng.0c03553.

[45] Mood Mohan, Jay D. Keasling, Blake A. Simmons, and Seema Singh. *In silico* COSMO-RS predictive screening of ionic liquids for the dissolution of plastic. *Green Chemistry*, 24(10):4140–4152, 2022. doi: 10.1039/d1gc03464b. URL https://doi.org/10.1039%2Fd1gc03464b.

[46] Ahmad S. Darwish, Tarek Lemaoui, Jawaher AlYammahi, Hanifa Taher, Yacine Benguerba, Fawzi Banat, and Inas M. AlNashef. Molecular insights into potential hydrophobic deep eutectic solvents for furfural extraction guided by cosmo-rs and machine learning. *Journal of Molecular Liquids*, 379, 2023. doi: 10.1016/j.molliq.2023.121631. URL https://www.scopus.com/inward/record.uri?eid=2-s2.0-85151788205&doi=10.1016%2fj.molliq.2023.121631&partnerID=40&md5=c84e920dce078cfdc369fe445a39b808. Cited by: 0.

[47] Mood Mohan, Blake A. Simmons, Kenneth L. Sale, and Seema Singh. Multi-scale molecular simulations for the solvation of lignin in ionic liquids. *Scientific Reports*, 13(1), 2023. doi: 10.1038/s41598-022-25372-2. URL https://www.scopus.com/inward/record.uri?eid=2-s2.0-85145870222&doi=10.1038%2fs41598-022-25372-2&partnerID=40&md5=a7d32a508f2cbfb346dc01df87fe2668. Cited by: 1; All Open Access, Gold Open Access, Green Open Access.

[48] Joachim Gross and Gabriele Sadowski. Perturbed-Chain SAFT: An Equation of State Based on a Perturbation Theory for Chain Molecules. *Industrial & Engineering Chemistry Research*, 40:1244–1260, 2 2001. ISSN 0888-5885. doi: 10.1021/ie0003887. URL https://pubs.acs.org/doi/10.1021/ie0003887.

[49] Joachim Gross and Gabriele Sadowski. Application of the Perturbed-Chain SAFT Equation of State to Associating Systems. *Industrial & Engineering Chemistry Research*, 41: 5510–5515, 10 2002. ISSN 0888-5885. doi: 10.1021/ie010954d. URL https://pubs.acs.org/doi/10.1021/ie010954d.

[50] Theodora Spyriouni, Xenophon Krokidis, and Ioannis G. Economou. Thermodynamics of pharmaceuticals: Prediction of solubility in pure and mixed solvents with PC-SAFT. *Fluid Phase Equilibria*, 302(1-2):331–337, 2011. ISSN 0378-3812. doi: 10.1016/j.fluid.2010.08.029.

[51] Samane Zarei Mahmoudabadi and Gholamreza Pazuki. A predictive PC-SAFT EOS based on COSMO for pharmaceutical compounds. *Scientific Reports*, 11:6405, 3 2021. ISSN 2045-2322. doi: 10.1038/s41598-021-85942-8.

[52] Lawien F. Zubeir, Christoph Held, Gabriele Sadowski, and Maaike C. Kroon. Pc-saft modeling of co2 solubilities in deep eutectic solvents. *The Journal of Physical Chemistry B*, 120(9):2300–2310, 2016. doi: 10.1021/acs.jpcb.5b07888. URL https://doi.org/10.1021/acs.jpcb.5b07888. PMID: 26814164.

[53] Carin H.J.T. Dietz, Annika Erve, Maaike C. Kroon, Martin van Sint Annaland, Fausto Gallucci, and Christoph Held. Thermodynamic properties of hydrophobic deep eutectic solvents and solubility of water and HMF in them: Measurements and PC-SAFT modeling. *Fluid Phase Equilibria*, 489:75–82, 6 2019. ISSN 03783812. doi: 10.1016/j.fluid.2019.02.010.

[54] Bruno Sepúlveda-Orellana, Nicolás F. Gajardo-Parra, Hoang T. Do, José R. Pérez-Correa, Christoph Held, Gabriele Sadowski, and Roberto I. Canales. Measurement and PC-SAFT Modeling of the Solubility of Gallic Acid in Aqueous Mixtures of Deep Eutectic Solvents. *Journal of Chemical & Engineering Data*, 66:958–967, 2 2021. ISSN 0021-9568. doi: 10.1021/acs.jced.0c00784.

[55] Thomas Gerlach, Simon Müller, Andrés González de Castilla, and Irina Smirnova. An open source COSMO-RS implementation and parameterization supporting the efficient implementation of multiple segment descriptors. *Fluid Phase Equilibria*, 560: 113472, sep 2022. doi: 10.1016/j.fluid.2022.113472. URL https://doi.org/10.1016%2Fj.fluid.2022.113472.

[56] Manuel Díaz de los Ríos and Eduardo Hernández Ramos. Determination of the Hansen solubility parameters and the Hansen sphere radius with the aid of the solver add-in of Microsoft Excel. *SN Appl. Sci.*, 2(4), April 2020.

[57] Didier Mathieu. Pencil and Paper Estimation of Hansen Solubility Parameters. *ACS Omega*, 3(12):17049–17056, 2018. ISSN 2470-1343. doi: 10.1021/acsomega.8b02601.

[58] O. F. Solomon and I. Z. Ciută. Détermination de la viscosité intrinsèque de solutions de polymères par une simple détermination de la viscosité. *Journal of Applied Polymer Science*, 6(24):683–686, November 1962. ISSN 00218995, 10974628. doi: 10.1002/app.1962.070062414. URL https://onlinelibrary.wiley.com/doi/10.1002/app.1962.070062414.

[59] Ovidiu Segarceanu and Minodora Leca. Improved method to calculate Hansen solubility parameters of a polymer. *Progress in Organic Coatings*, 31(4):307–310, August 1997. ISSN 03009440. doi: 10.1016/S0300-9440(97)00088-X. URL https://linkinghub.elsevier.com/retrieve/pii/S030094409700088X.

[60] Pilar Bustamante, Javier Navarro-Lupión, and Begoña Escalera. A new method to determine the partial solubility parameters of polymers from intrinsic viscosity. *European Journal of Pharmaceutical Sciences*, 24(2-3):229–237, February 2005. ISSN 09280987. doi: 10.1016/j.ejps.2004.10.012. URL https://linkinghub.elsevier.com/retrieve/pii/S0928098704002647.

[61] Jason Howell, Miranda Roesing, and David Boucher. A Functional Approach to Solubility Parameter Computations. *The Journal of Physical Chemistry B*, 121(16):4191–4201, April 2017. ISSN 1520-6106, 1520-5207. doi: 10.1021/acs.jpcb.7b01537. URL https://pubs.acs.org/doi/10.1021/acs.jpcb.7b01537.

[62] Thomas Lindvig, Michael L Michelsen, and Georgios M Kontogeorgis. A Flory–Huggins model based on the Hansen solubility parameters. *Fluid Phase Equilibria*, 203(1-2):247–260, 2002. ISSN 0378-3812. doi: 10.1016/s0378-3812(02)00184-x.

[63] Hassan Modarresi, Elisa Conte, Jens Abildskov, Rafiqul Gani, and Peter Crafts. Model-Based Calculation of Solid Solubility for Solvent Selection: A Review. *Industrial & Engineering Chemistry Research*, 47(15):5234–5242, 2008. ISSN 0888-5885. doi: 10.1021/ie0716363.

[64] Andreas Klamt. Conductor-like Screening Model for Real Solvents: A New Approach to the Quantitative Calculation of Solvation Phenomena. *The Journal of Physical Chemistry*, 99(7):2224–2235, 1995. ISSN 0022-3654. doi: 10.1021/j100007a062.

[65] Andreas Klamt, Gerard J. P. Krooshof, and Ross Taylor. COSMOSPACE: Alternative to conventional activity-coefficient models. *AIChE Journal*, 48(10):2332–2349, 2002. ISSN 0001-1541. doi: 10.1002/aic.690481023.

[66] A. J. Staverman. The entropy of high polymer solutions. Generalization of formulae. *Recueil des Travaux Chimiques des Pays-Bas*, 69(2):163–174, 1950. ISSN 0165-0513. doi: 10.1002/recl.19500690203.

[67] Thomas Brouwer and Boelo Schuur. Model Performances Evaluated for Infinite Dilution Activity Coefficients Prediction at 298.15 K. *Industrial & Engineering Chemistry Research*, 58(20):8903–8914, 2019. ISSN 0888-5885. doi: 10.1021/acs.iecr.9b00727.

[68] Jean-Paul Ebejer, Garrett M Morris, and Charlotte M Deane. Freely available conformer generation methods: how good are they? *J. Chem. Inf. Model.*, 52(5):1146–1158, May 2012.

[69] Jeffrey M Blaney and J Scott Dixon. Distance geometry in molecular modeling. In *Reviews in Computational Chemistry*, pages 299–335. John Wiley & Sons, Inc., Hoboken, NJ, USA, January 2007.

[70] Frank Neese. The ORCA program system. *WIREs Computational Molecular Science*, 2 (1):73–78, jun 2011. doi: 10.1002/wcms.81. URL https://doi.org/10.1002%2Fwcms.81.

[71] Frank Neese. Software update: the ORCA program system, version 4.0. *WIREs Computational Molecular Science*, 8(1), jul 2017. doi: 10.1002/wcms.1327. URL https://doi.org/10.1002%2Fwcms.1327.

[72] Frank Neese, Frank Wennmohs, Ute Becker, and Christoph Riplinger. The ORCA quantum chemistry program package. *The Journal of Chemical Physics*, 152(22):224108, jun 2020. doi: 10.1063/5.0004608. URL https://doi.org/10.1063%2F5.0004608.

[73] Martin Klajmon. Purely Predicting the Pharmaceutical Solubility: What to Expect from PC-SAFT and COSMO-RS? *Molecular Pharmaceutics*, 19(11):4212–4232, 2022. ISSN 1543-8384. doi: 10.1021/acs.molpharmaceut.2c00573.

[74] Samane Zarei Mahmoudabadi and Gholamreza Pazuki. A predictive PC-SAFT EOS based on COSMO for pharmaceutical compounds. *Scientific Reports*, 11:6405, 3 2021. ISSN 2045-2322. doi: 10.1038/s41598-021-85942-8.

[75] John M Prausnitz, Ruediger N Lichtenthaler, and Edmundo Gomes de Azevedo. *Molecular Thermodynamics of Fluid-Phase Equilibria*. Prentice Hall, Philadelphia, PA, 3 edition, October 1998.

[76] João A.P. Coutinho, Simon I. Andersen, and Erling H. Stenby. Evaluation of activity coefficient models in prediction of alkane solid-liquid equilibria. *Fluid Phase Equilibria*, 103(1):23–39, 1995. ISSN 0378-3812. doi: 10.1016/0378-3812(94)02600-6.

[77] Dinis O. Abranches, Mónia A. R. Martins, Liliana P. Silva, Nicolas Schaeffer, Simão P. Pinho, and João A. P. Coutinho. Phenolic hydrogen bond donors in the formation of non-ionic deep eutectic solvents: the quest for type V DES. *Chemical Communications*, 55(69):10253–10256, 2019. ISSN 1359-7345. doi: 10.1039/c9cc04846d.

[78] Ahmad Alhadid, Christian Jandl, Liudmila Mokrushina, and Mirjana Minceva. Experimental Investigation and Modeling of Cocrystal Formation in L-Menthol/Thymol Eutectic System. *Crystal Growth & Design*, 21(11):6083–6091, 2021. ISSN 1528-7483. doi: 10.1021/acs.cgd.1c00306.

[79] Nicolas Schaeffer, Dinis O Abranches, Liliana P Silva, Mónia A R Martins, Pedro J Carvalho, Olga Russina, Alessandro Triolo, Laurent Paccou, Yannick Guinet, Alain Hedoux, and João A P Coutinho. Non-Ideality in Thymol + Menthol Type V Deep Eutectic Solvents. *ACS Sustainable Chemistry & Engineering*, 9(5):2203–2211, 2021. ISSN 2168-0485. doi: 10.1021/acssuschemeng.0c07874.

[80] Ahmad Alhadid, Christian Jandl, Liudmila Mokrushina, and Mirjana Minceva. Cocrystal Formation in l-Menthol/Phenol Eutectic System: Experimental Study and Thermodynamic Modeling. *Crystal Growth & Design*, 22(6):3973–3980, 2022. ISSN 1528-7483. doi: 10.1021/acs.cgd.2c00362.

[81] Ahmad Alhadid, Christian Jandl, Liudmila Mokrushina, and Mirjana Minceva. Non-ideality and cocrystal formation in l-menthol/xylenol eutectic systems. *Journal of Molecular Liquids*, 367:120582, 2022. ISSN 0167-7322. doi: 10.1016/j.molliq.2022.120582.

[82] Nobuo Nakamura, Hiroshi Suga, and Syûzô Seki. Calorimetric Study on Orientationally Disordered Crystals. Cyclohexene Oxide and Cyclohexanone. *Bulletin of the Chemical Society of Japan*, 53(10):2755–2761, oct 1980. doi: 10.1246/bcsj.53.2755. URL https://doi.org/10.1246%2Fbcsj.53.2755.

[83] Benjamin Sanchez-Lengeling, Loïc M. Roch, José Darío Perea, Stefan Langner, Christoph J. Brabec, and Alán Aspuru-Guzik. A Bayesian Approach to Predict Solubility Parameters. *Advanced Theory and Simulations*, 2(1):1800069, 2019. ISSN 2513-0390. doi: 10.1002/adts.201800069.

[84] José Pedro Wojeicchowski, Ana M. Ferreira, Tifany Okura, Marlus Pinheiro Rolemberg, Marcos R. Mafra, and João A. P. Coutinho. Using COSMO-RS to Predict Hansen Solubility Parameters. *Industrial & Engineering Chemistry Research*, 61(42):15631–15638, 2022. ISSN 0888-5885. doi: 10.1021/acs.iecr.2c01592.

[85] Máté Mihalovits. Determination of the Hansen solubility parameters from solubility data using an improved evaluation approach, the concentric spheroids method. *Journal of Molecular Liquids*, 364:119911, 2022. ISSN 0167-7322. doi: 10.1016/j.molliq.2022.119911.

[86] Baptiste Bouillot, Sébastien Teychené, and Béatrice Biscans. An evaluation of thermodynamic models for the prediction of drug and drug-like molecule solubility in organic solvents. *Fluid Phase Equilibria*, 309(1):36–52, 2011. ISSN 0378-3812. doi: 10.1016/j.fluid.2011.06.032.

[87] Bruno Sepúlveda-Orellana, Nicolás F. Gajardo-Parra, Hoang T. Do, José R. Pérez-Correa, Christoph Held, Gabriele Sadowski, and Roberto I. Canales. Measurement and PC-SAFT Modeling of the Solubility of Gallic Acid in Aqueous Mixtures of Deep Eutectic Solvents. *Journal of Chemical & Engineering Data*, 66(2):958–967, 2021. ISSN 0021-9568. doi: 10.1021/acs.jced.0c00784.

[88] Samane Zarei Mahmoudabadi and Gholamreza Pazuki. Application of PC-SAFT EOS for Pharmaceuticals: Solubility, Co-Crystal, and Thermodynamic Modeling. *Journal of Pharmaceutical Sciences*, 110(6):2442–2451, 2021. ISSN 0022-3549. doi: 10.1016/j.xphs.2020.12.035.

[89] Mood Mohan, Tamal Banerjee, and Vaibhav V. Goud. COSMO-RS-Based Screening of Antisolvents for the Separation of Sugars from Ionic Liquids: Experimental and Molecular Dynamic Simulations. *ACS Omega*, 3(7):7358–7370, jul 2018. doi: 10.1021/acsomega.8b00253. URL https://doi.org/10.1021%2Facsomega.8b00253.

[90] Costas Panayiotou. Partial Solvation Parameters and Mixture Thermodynamics. *The Journal of Physical Chemistry B*, 116(24):7302–7321, jun 2012. doi: 10.1021/jp303053u. URL https://doi.org/10.1021%2Fjp303053u.

[91] Spyros Mastrogeorgopoulos, Vassily Hatzimanikatis, and Costas Panayiotou. Toward a Simple Predictive Molecular Thermodynamic Model for Bulk Phases and Interfaces. *Industrial & Engineering Chemistry Research*, 56(38):10900–10910, sep 2017. doi: 10.1021/acs.iecr.7b02286. URL https://doi.org/10.1021%2Facs.iecr.7b02286.

[92] Jinbo Ouyang, Limin Zhou, Zhirong Liu, Saijin Xiao, Xin Huang, and Jerry Y.Y. Heng. Solubility determination and modelling of benzamide in organic solvents at temperatures from 283.15 K and 323.15 K, and ternary phase diagrams of benzamide-benzoic acid cocrystals in ethanol at 298.15 K. *Journal of Molecular Liquids*, 286:110885, 2019. ISSN 0167-7322. doi: 10.1016/j.molliq.2019.110885.

[93] Théophile Gaudin, Adrien Benazzouz, and Jean-Marie Aubry. Robust definition and prediction of dispersive Hansen solubility parameter $\delta_D$ with COSMO-RS. *Computational and Theoretical Chemistry*, 1221:114023, 2023. ISSN 2210-271X. doi: 10.1016/j.comptc.2023.114023.

[94] Elisabeth Bosch, Fernando Rived, and Martí Rosés. Solute–solvent and solvent–solvent interactions in binary solvent mixtures. Part 4. Preferential solvation of solvatochromic indicators in mixtures of 2-methylpropan-2-ol with hexane, benzene, propan-2-ol, ethanol and methanol. *Journal of the Chemical Society, Perkin Transactions 2*, 0(10):2177–2184, 1996. ISSN 0300-9580. doi: 10.1039/p29960002177.

[95] Andreas Klamt, Frank Eckert, Martin Hornig, Michael E. Beck, and Thorsten Bürger. Prediction of aqueous solubility of drugs and pesticides with COSMO-RS. *Journal of Computational Chemistry*, 23(2):275–281, 2002. ISSN 0192-8651. doi: 10.1002/jcc.1168.

[96] Ioannis Tsivintzelis, Ioannis G. Economou, and Georgios M. Kontogeorgis. Modeling the solid–liquid equilibrium in pharmaceutical-solvent mixtures: Systems with complex hydrogen bonding behavior. *AIChE Journal*, 55(3):756–770, 2009. ISSN 0001-1541. doi: 10.1002/aic.11716.

[97] Meera C Singh, Priyanka Nangre, Nikita N Bagade, and Rukhsana A Rub. Formulation and Evaluation of Microemulsion of Curcumin in Thymol-Menthol Carrier System. *Journal of Pharmaceutical Research International*, pages 420–434, 2021. doi: 10.9734/jpri/2021/v33i60b34637.

[98] Costas Panayiotou, Ioannis Zuburtikudis, and Vassily Hatzimanikatis. 110th Anniversary: From Solubility Parameters to Predictive Equation-of-State Modeling. *Industrial & Engineering Chemistry Research*, 58(28):12787–12800, jun 2019. doi: 10.1021/acs.iecr.9b02908. URL https://doi.org/10.1021%2Facs.iecr.9b02908.

[99] Costas Panayiotou. Thermodynamic characterization of polymers. *Polymer*, 136:47–61, 2018. ISSN 0032-3861. doi: 10.1016/j.polymer.2017.12.047.

[100] Dimitra Lazidou, Spyros Mastrogeorgopoulos, and Costas Panayiotou. Thermodynamic characterization of ionic liquids. *Journal of Molecular Liquids*, 277:10–21, 2019. ISSN 0167-7322. doi: 10.1016/j.molliq.2018.12.023.

[101] Costas Panayiotou and Vassily Hatzimanikatis. The solubility parameters of carbon dioxide and ionic liquids: Are they an enigma? *Fluid Phase Equilibria*, 527:112828, 2021. ISSN 0378-3812. doi: 10.1016/j.fluid.2020.112828.

[102] Manuel J. Louwerse, Ana Maldonado, Simon Rousseau, Chloe Moreau-Masselon, Bernard Roux, and Gadi Rothenberg. Revisiting Hansen Solubility Parameters by Including Thermodynamics. *Chemphyschem*, 18(21):2999–3006, 2017. ISSN 1439-4235. doi: 10.1002/cphc.201700408.

[103] David S. Boucher. Solubility parameters and solvent affinities for polycaprolactone: A comparison of methods. *Journal of Applied Polymer Science*, 137(30):48908, 2020. ISSN 0021-8995. doi: 10.1002/app.48908.

[104] F. Hecht. New development in FreeFEM++. *Journal of Numerical Mathematics*, 20(3-4):251–266, 2012. ISSN 1570-2820. doi: 10.1515/jnum-2012-0013.

[105] Sang Hyun Lee and Sun Bok Lee. The Hildebrand solubility parameters, cohesive energy densities and internal energies of 1-alkyl-3-methylimidazolium-based room temperature ionic liquids. *Chemical Communications*, 0(27):3469–3471, 2005. ISSN 1359-7345. doi: 10.1039/b503740a.

[106] Vishnu Malpani, Pralhad A. Ganeshpure, and Pradip Munshi. Determination of Solubility Parameters for the p-Xylene Oxidation Products. *Industrial & Engineering Chemistry Research*, 50(4):2467–2472, 2011. ISSN 0888-5885. doi: 10.1021/ie101623c.

[107] Piyarat Weerachanchai, Zhengjian Chen, Susanna Su Jan Leong, Matthew Wook Chang, and Jong-Min Lee. Hildebrand solubility parameters of ionic liquids: Effects of ionic liquid type, temperature and DMA fraction in ionic liquid. *Chemical Engineering Journal*, 213:356–362, 2012. ISSN 1385-8947. doi: 10.1016/j.cej.2012.10.012.

[108] Piyarat Weerachanchai, Yuewen Wong, Kok Hwa Lim, Timothy Thatt Yang Tan, and Jong-Min Lee. Determination of Solubility Parameters of Ionic Liquids and Ionic Liquid/Solvent Mixtures from Intrinsic Viscosity. *ChemPhysChem*, 15(16):3580–3591, 2014. ISSN 1439-7641. doi: 10.1002/cphc.201402345.

[109] Yuewen Wong, Zheng Jian Chen, Timothy Thatt Yang Tan, and Jong-Min Lee. Hildebrand Solubility Parameters of Amidium Ionic Liquids. *Industrial & Engineering Chemistry Research*, 54(48):12150–12155, 2015. ISSN 0888-5885. doi: 10.1021/acs.iecr.5b02705.

[110] A.M. Seuvre and M. Mathlouthi. Solutions properties and solute–solvent interactions in ternary sugar–salt–water solutions. *Food Chemistry*, 122(2):455–461, 2010. ISSN 0308-8146. doi: 10.1016/j.foodchem.2009.04.101.

[111] E. H. Catsiff. A comment on solomon and ciută's single-point method for determining intrinsic viscosity. *Journal of Applied Polymer Science*, 7(6):S37–S38, 1963. ISSN 0021-8995. doi: 10.1002/app.1963.070070632.

[112] Jon Herman and Will Usher. SALib: An open-source Python library for Sensitivity Analysis. *The Journal of Open Source Software*, 2(9):97, 2017. doi: 10.21105/joss.00097.

[113] Christian Wohlfarth. *Viscosity of pure organic liquids and binary liquid mixtures*. Landolt-Börnstein: Numerical Data and Functional Relationships in Science and Technology - New Series. Springer, Berlin, Germany, 2009 edition, January 2009.

[114] U. Onken, J. Rarey-Nies, and J. Gmehling. The Dortmund Data Bank: A computerized system for retrieval, correlation, and prediction of thermodynamic properties of mixtures. *International Journal of Thermophysics*, 10(3):739–747, may 1989. doi: 10.1007/bf00507993. URL https://doi.org/10.1007%2Fbf00507993.

[115] William M. Haynes, editor. *CRC Handbook of Chemistry and Physics*. CRC Press, jun 2014. doi: 10.1201/b17118. URL https://doi.org/10.1201%2Fb17118.

[116] Ron Wehrens, Hein Putter, and Lutgarde M.C Buydens. The bootstrap: a tutorial. *Chemometrics and Intelligent Laboratory Systems*, 54(1):35–52, 2000. ISSN 0169-7439. doi: 10.1016/s0169-7439(00)00102-7.

[117] Manuel A.V. Ribeiro da Silva, José M.S. Fonseca, Rui P.B.M. Carvalho, and Manuel J.S. Monte. Thermodynamic study of the sublimation of six halobenzoic acids. *The Journal of Chemical Thermodynamics*, 37(3):271–279, 2005. ISSN 0021-9614. doi: https://doi.org/10.1016/j.jct.2004.09.005. URL https://www.sciencedirect.com/science/article/pii/S0021961404001909.

[118] William E. Acree. Thermodynamic properties of organic compounds: enthalpy of fusion and melting point temperature compilation. *Thermochimica Acta*, 189(1):37–56, 1991. ISSN 0040-6031. doi: https://doi.org/10.1016/0040-6031(91)87098-H. URL https://www.sciencedirect.com/science/article/pii/004060319187098H.

[119] James S. Chickos, William E. Acree, and Joel F. Liebman. *NIST Chemistry WebBook, NIST Standard Reference Database 69*, chapter Heat of Fusion data. National Institute of Standards and Technology, 1997.

[120] Eugene S. Domalski and Elizabeth D. Hearing. Heat Capacities and Entropies of Organic Compounds in the Condensed Phase. Volume III. *Journal of Physical and Chemical Reference Data*, 25(1):1, jan 1996. doi: 10.1063/1.555985. URL https://doi.org/10.1063%2F1.555985.

[121] W.V. Steele, R.D. Chirico, I.A. Hossenlopp, A. Nguyen, N.K. Smith, and B.E. Gammon. The thermodynamic properties of the five benzoquinolines. *The Journal of Chemical Thermodynamics*, 21(1):81–107, 1989. ISSN 0021-9614. doi: 10.1016/0021-9614(89)90010-4.

[122] Maria Victoria Roux, Manuel Temprado, and James S. Chickos. Vaporization, fusion and sublimation enthalpies of the dicarboxylic acids from C4 to C14 and C16. *The Journal of Chemical Thermodynamics*, 37(9):941–953, sep 2005. doi: 10.1016/j.jct.2004.12.011. URL https://doi.org/10.1016%2Fj.jct.2004.12.011.

[123] Sponsored by AIChE Design Institute for Physical Properties. Design Institute for Physical Property Research/AIChE, 2021. ISBN N/A. URL https://app.knovel.com/hotlink/toc/id:kpDIPPRPF7/dippr-project-801-full/dippr-project-801-full.

[124] Defoe C. Ginnings and George T. Furukawa. Heat capacity standards for the range 14 to 1200°k. *Journal of the American Chemical Society*, 75(3):522–527, 1953. doi: 10.1021/ja01099a004. URL https://doi.org/10.1021/ja01099a004.

[125] Vojtěch Štejfa, Michal Fulem, Květoslav Růžička, and Ctirad Červinka. Thermodynamic study of selected monoterpenes ii. *The Journal of Chemical Thermodynamics*, 79:272–279, 2014. ISSN 0021-9614. doi: https://doi.org/10.1016/j.jct.2013.12.012. URL https://www.sciencedirect.com/science/article/pii/S0021961413004771.

[126] E. V. Agafonova, Yu. V. Moshchenskii, and M. L. Tkachenko. Determining the main thermodynamic parameters of caffeine melting by means of DSC. *Russian Journal of Physical Chemistry A*, 86(6):1035–1037, may 2012. doi: 10.1134/s0036024412060027. URL https://doi.org/10.1134%2Fs0036024412060027.

[127] E.W. Washburn. *International Critical Tables of Numerical Data, Physics, Chemistry and Technology (1st Electronic Edition)*. Knovel, 1926 - 1930;2003. ISBN N/A. URL https://app.knovel.com/hotlink/toc/id:kpICTNDPC4/international-critical/international-critical.

[128] R.A. Fugita, D.A. Gálico, Renan Guerra, Glauco Perpetuo, Oswaldo Treu-Filho, M.S. Galhiane, R.A. Mendes, and Gilbert Bannach. Thermal behaviour of curcumin. *Braz. J. Therm. Anal.*, 1:19–23, 01 2012.

[129] Wanya Li, Yiming Ma, Yang Yang, Shijie Xu, Peng Shi, and Songgu Wu. Solubility measurement, correlation and mixing thermodynamics properties of dapsone in twelve mono solvents. *Journal of Molecular Liquids*, 280:175–181, 2019. ISSN 0167-7322.

[130] Ivo B. Rietveld, Maria Barrio, Nestor Veglio, Philippe Espeau, Josep Lluis Tamarit, and René Céolin. Temperature and composition-dependent properties of the two-component system d- and l-camphor at 'ordinary' pressure. *Thermochimica Acta*, 511 (1):43–50, 2010. ISSN 0040-6031. doi: https://doi.org/10.1016/j.tca.2010.07.023. URL https://www.sciencedirect.com/science/article/pii/S0040603110002789.

[131] Artem O. Surov, Irina V. Terekhova, Annette Bauer-Brandl, and German L. Perlovich. Thermodynamic and structural aspects of some fenamate molecular crystals. *Crystal Growth & Design*, 9(7):3265–3272, 2009. doi: 10.1021/cg900002q. URL https://doi.org/10.1021/cg900002q.

[132] Svava Ósk Jónsdóttir, Stephen A. Cooke, and Eugénia A. Macedo. Modeling and measurements of solid–liquid and vapor–liquid equilibria of polyols and carbohydrates in aqueous solution. *Carbohydrate Research*, 337(17):1563–1571, sep 2002. doi: 10.1016/s0008-6215(02)00213-6. URL https://doi.org/10.1016%2Fs0008-6215%2802%2900213-6.

[133] David J. Good and Naír Rodríguez-Hornedo. Solubility Advantage of Pharmaceutical Cocrystals. *Crystal Growth & Design*, 9(5):2252–2264, mar 2009. doi: 10.1021/cg801039j. URL https://doi.org/10.1021%2Fcg801039j.

[134] Yeong Zen Chua, Hoang Tam Do, Christoph Schick, Dzmitry Zaitsau, and Christoph Held. New experimental melting properties as access for predicting amino-acid solubility. *RSC Advances*, 8(12):6365–6372, 2018. ISSN 2046-2069. doi: 10.1039/c8ra00334c.

[135] F. Cilurzo, E. Alberti, P. Minghetti, C.G.M. Gennari, A. Casiraghi, and L. Montanari. Effect of drug chirality on the skin permeability of ibuprofen. *International Journal of Pharmaceutics*, 386(1-2):71–76, feb 2010. doi: 10.1016/j.ijpharm.2009.10.053. URL https://doi.org/10.1016%2Fj.ijpharm.2009.10.053.

[136] Carola M. Wassvik, Anders G. Holmén, Christel A.S. Bergström, Ismael Zamora, and Per Artursson. Contribution of solid-state properties to the aqueous solubility of drugs. *European Journal of Pharmaceutical Sciences*, 29(3-4):294–305, nov 2006. doi: 10.1016/j.ejps.2006.05.013. URL https://doi.org/10.1016%2Fj.ejps.2006.05.013.

[137] Mónia A. R. Martins, Emanuel A. Crespo, Paula V. A. Pontes, Liliana P. Silva, Mark Bülow, Guilherme J. Maximo, Eduardo A. C. Batista, Christoph Held, Simão P. Pinho, and João A. P. Coutinho. Tunable Hydrophobic Eutectic Solvents Based on Terpenes and Monocarboxylic Acids. *ACS Sustainable Chemistry & Engineering*, 6(7):8836–8846, may 2018. doi: 10.1021/acssuschemeng.8b01203. URL https://doi.org/10.1021%2Facssuschemeng.8b01203.

[138] Li-Guo Kong, Zhi-Cheng Tan, Jian-Ting Mei, Li-Xian Sun, and Xin-He Bao. Thermodynamic studies of monuron. *Thermochimica Acta*, 414(2):131–135, 2004. ISSN 0040-6031. doi: https://doi.org/10.1016/j.tca.2003.12.007. URL https://www.sciencedirect.com/science/article/pii/S0040603103006841.

[139] Sandra Gracin and Ake C. Rasmuson. Polymorphism and crystallization of p-aminobenzoic acid. *Crystal Growth & Design*, 4(5):1013–1023, 2004. doi: 10.1021/cg049954h. URL https://doi.org/10.1021/cg049954h.

[140] Fátima L. Mota, Aristides P. Carneiro, António J. Queimada, Simão P. Pinho, and Eugénia A. Macedo. Temperature and solvent effects in the solubility of some pharmaceutical compounds: Measurements and modeling. *European Journal of Pharmaceutical Sciences*, 37(3):499–507, 2009. ISSN 0928-0987. doi: https://doi.org/10.1016/j.ejps.2009.04.009. URL https://www.sciencedirect.com/science/article/pii/S0928098709001304.

[141] R. J. L. Andon, J. F. Counsell, E. F. G. Herington, and J. F. Martin. Thermodynamic properties of organic oxygen compounds. part 7.—calorimetric study of phenol from 12 to 330°k. *Trans. Faraday Soc.*, 59:830–835, 1963. doi: 10.1039/TF9635900830. URL http://dx.doi.org/10.1039/TF9635900830.

[142] Latifa Chebil, Catherine Humeau, Julie Anthoni, François Dehez, Jean-Marc Engasser, and Mohamed Ghoul. Solubility of Flavonoids in Organic Solvents. *Journal of Chemical & Engineering Data*, 52(5):1552–1556, jul 2007. doi: 10.1021/je7001094. URL https://doi.org/10.1021%2Fje7001094.

[143] M.A. Peña, B. Escalera, A. Reíllo, A.B. Sánchez, and P. Bustamante. Thermodynamics of cosolvent action: Phenacetin, salicylic acid and probenecid. *Journal of Pharmaceutical Sciences*, 98(3):1129–1135, mar 2009. doi: 10.1002/jps.21497. URL https://doi.org/10.1002%2Fjps.21497.

[144] Xiangji Liao, Xiuqing Li, Yujun Han, Jun Song, Yingjie Gao, Ao Yang, Yan Zhu, and Weiping Luo. Measurement and Correlation for the Solubility of Adipic Acid and Succinic

Acid in Glutaric Acid + Cyclohexanone and Glutaric Acid + Acetic Acid Mixtures. *Journal of Chemical & Engineering Data*, 62(10):3473–3482, 2017. ISSN 0021-9568. doi: 10.1021/acs.jced.7b00468.

[145] Sérgio M. Vilas-Boas, Isabella W. Cordova, Dinis O. Abranches, João A. P. Coutinho, Olga Ferreira, and Simão P. Pinho. Modeling the Solubility of Monoterpenoids with Hybrid and Predictive Thermodynamic Tools. *Industrial & Engineering Chemistry Research*, 62(12):5326–5335, 2023. ISSN 0888-5885. doi: 10.1021/acs.iecr.2c03991.

[146] Xin Tong, Delani Woods, William E. Acree, and Michael H Abraham. Updated Abraham model correlations for correlating solute transfer into dry butanone and dry cyclohexanone solvents. *Physics and Chemistry of Liquids*, 56(5):571–583, 2018. ISSN 0031-9104. doi: 10.1080/00319104.2017.1354377.

[147] Fan Lihua, Ma Peisheng, and Xiang Zhengle. Measurement and Correlation for Solubility of Adipic Acid in Several Solvents. *Chinese Journal of Chemical Engineering*, 15(1): 110–114, 2007. ISSN 1004-9541. doi: https://doi.org/10.1016/S1004-9541(07)60042-1. URL `https://www.sciencedirect.com/science/article/pii/S1004954107600421`.

[148] Weiwei Song, Peisheng MA, Lihua Fan, and Zhengle Xiang. Solubility of Glutaric Acid in Cyclohexanone, Cyclohexanol, Their Five Mixtures and Acetic Acid. *Chinese Journal of Chemical Engineering*, 15(2):228–232, 2007. ISSN 1004-9541. doi: 10.1016/s1004-9541(07)60063-9.

# Appendix

## A. Chemicals

Table A.1.: Specifications of the solvents used in this work. Molar mass ($M$), CAS number, supplier and Hansen solubility parameters obtained from literature [1] are included. $\delta_d$, $\delta_d$ and $\delta_d$ are expressed in $MPa^{0.5}$.

| Solvent | $M$ / $g \cdot mol^{-1}$ | CAS | Supplier | $\delta_d$ | $\delta_p$ | $\delta_h$ |
|---|---|---|---|---|---|---|
| 1,4-Dioxane | 88.11 | 123-91-1 | Merck | 17.5 | 1.8 | 9 |
| 2-Propanol | 60.1 | 67-63-0 | Merck | 15.8 | 6.1 | 16.4 |
| Acetic acid | 60.05 | 64-19-7 | Merck | 14.5 | 8 | 13.4 |
| Acetic anhydride | 102.09 | 108-24-7 | Merck | 16 | 11.7 | 10.2 |
| Acetone | 58.08 | 67-64-1 | Merck | 15.5 | 10.4 | 7 |
| Acetonitrile | 41.05 | 75-05-8 | Merck | 15.3 | 18 | 6.1 |
| Chlorobenzene | 112.56 | 108-90-7 | Merck | 19 | 4.3 | 2 |
| Chloroform | 119.38 | 865-49-6 | Merck | 17.8 | 3.1 | 5.7 |
| Diethyl ether | 74.12 | 60-29-7 | Merck | 14.5 | 2.9 | 4.6 |
| Dimethyl formamide (DMF) | 73.09 | 68-12-2 | Merck | 17.4 | 13.7 | 11.3 |
| Dimethyl sulfoxide (DMSO) | 78.13 | 67-68-5 | Merck | 18.4 | 16.4 | 10.2 |
| Ethanol | 46.08 | 64-17-5 | Merck | 15.8 | 8.8 | 19.4 |
| Ethyl acetate | 88.11 | 141-78-6 | Winkler | 15.8 | 5.3 | 7.2 |
| Ethylene glycol | 62.07 | 107-21-1 | Merck | 17 | 11 | 26 |
| Formic acid | 46.03 | 64-18-6 | Merck | 14.3 | 11.9 | 16.6 |
| Methanol | 32.04 | 67-56-1 | Merck | 14.7 | 12.3 | 22.3 |
| Dichloromethane | 84.93 | 75-09-2 | Merck | 17 | 7.3 | 7.1 |
| Tetrahydrofuran (THF) | 72.11 | 109-99-9 | Merck | 16.8 | 5.7 | 8 |
| Toluene | 92.14 | 108-88-3 | Merck | 18 | 1.4 | 2 |
| Water | 18.01 | 7732-18-5 | Merck | 15.5 | 16 | 42.3 |

# B. Functional solubility parameters (FSP)

While HSP theory is widely used for assisting the selection of solvents for different applications, and the methods used to compute these parameters continue to be improved, there are criticisms to inherent considerations in this theory. Some of these are:

- Differences in experimental observations. It is a common issue that, when fitting the sphere to affinity data, the sphere may include solvents rated as "bad" and exclude "good".
- Different methods used for the optimization of the sphere of the same compound can result in important differences in the final result (values of $\delta_{\mathrm{d}}$, $\delta_{\mathrm{p}}$ and $\delta_{\mathrm{h}}$), even when feeding the same data set to the algorithm.
- In several cases solubility data must be reduced to a binary classification ("good" and "bad" solvents), losing information regarding the magnitude of the affinity between solute and solvent.
- An implicit assumption in approaching the solubility space as a sphere is that intermolecular interactions and dispersion, polar and hydrogen bonding contributions equally influence the solubility of the system. This assumption of isotropy in solubility behavior has been criticized by several authors [61, 102].

To address these problems, Howell et al. [61] developed a method that considers the solubility space as a function, i.e., at each point in the space defined by $\delta_{\mathrm{d}}$-$\delta_{\mathrm{p}}$-$\delta_{\mathrm{h}}$, a species A must dissolve in a solvent B by a certain amount, which can be zero. The method is based on assuming a solubility function, $f$, which is unknown, to which a value is assigned for each solvent. In this work, that value will be the intrinsic viscosity of the solute in each solvent, as reported by Boucher [103]. Thus, this function can be considered as the density of the solid formed by the points corresponding to each solvent in the Hansen space, and the functional solubility parameters (FSP) correspond to the coordinates of its center of mass. Fig. B.1 illustrates the basic concepts of the method, for a simplified space in two dimensions, $\delta_a - \delta_b$. The spatial domain $\Omega \in \mathbb{R}$ of the solubility function $f$ is considered as the convex envelope of the group of solvents used, i.e., those that are miscible with the solute in question. This creates an object with polyhedral faces, which will be triangulated, thus allowing the interpolation of $f$ throughout the domain. The method chosen for triangulation, as recommended in [61], is the Delaunay triangulation. Given a set of points, this method computes a list of simplices in terms of the indices of the nodes fed to the algorithm, and a list of triangular faces that constitute the boundaries of the triangulation. Once the .mesh file is obtained, it is used to interpolate the $f$ function over the entire domain. Then, this function is considered as a density function of the solid, and the center of mass of the solid is found by numerical integration. For this, we use the finite element software FreeFEM++ [104].

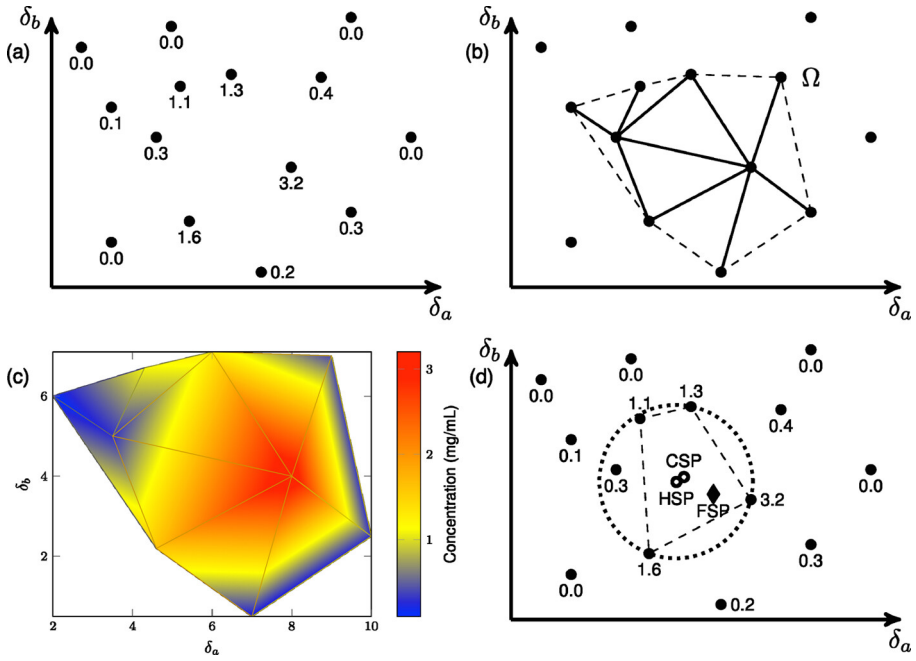


Figure B.1.: Illustration of the FSP methodology. (a) Dissolved concentrations of a solute in several solvents, represented as coordinates in the $\delta_a - \delta_b$ plane; (b) The $\Omega$ domain of the $f$ function is given by the Delaunay triangulation of the $(\delta_a - \delta_b)$ points with a concentration above zero; (c) interpolation of $f$ using the concentration values; (d) comparison between the FSP values and the ones obtained with other methods. Reproduced from [61].

# C. Intrinsic viscosity measurements

### On the applicability of Solomon-Ciuta (SC) equation for DES

To the best of the authors' knowledge, neither the intrinsic viscosity method nor the SC equation has been utilized to estimate the HSP of DES. However, several studies have employed the intrinsic viscosity method to calculate solubility parameters for ILs, yielding values comparable to those obtained through other conventional methods [105–109]. Unfortunately, these studies do not report the experimental viscosity data for those the $[\eta]$ values were obtained. Thus, validation of the SC equation for these systems, which could otherwise serve as a reference for molecules smaller than oligomers or polymers, is not possible.

The only study that the authors were able to find, which considers molecules of similar size, is the one from Seuvre and Mathlouthi [110]. The authors report intrinsic viscosity for different sugars in water (D-glucose, D-fructose, D-galactose, sucrose, and maltose), and in water + salts. Using the $\eta_{sp}/C$ vs. $C$ data, we compared the reported $[\eta]$ values, calculated via the extrapolation method, with the ones obtained using SC equation for several values of $C$. Fig. C.1a shows the relative error of the SC equation for these systems as a function of $C$. As expected, the error increases with increasing concentration. For around $C = 5\%$, the relative error averages a 7.2% considering the five systems (only the dilutions in water were considered). Moreover, the following expression can be used to estimate the expected error for the SC equation [111],

$$\% \text{ error} = 100[\eta]C\left(\frac{1}{6} - \beta\right) \tag{C.1}$$

where $\beta = 1/2 - K_H$, with $K_H$ the Huggins constant. Fig. C.1b shows the error of SC equation represented as contour lines, calculated by Eq. C.1, for different values of $K_H$ and $[\eta]C$. For the sugars above mentioned, average $[\eta]C$ values are $\sim$ 0.13, while for $K_H$ the values are $\sim$ 1.05 [110]. Locating these values in Fig. C.1b, one obtains errors between 6-8%, which is coherent with the average relative error mentioned above. Given that the structure of the mentioned sugars is similar to the DES precursors used in this study (rings that engage in hydrogen bonding interactions), it is reasonable to expect similar errors for the studied DESs.

The question that arises is what value of $C$ should be used for the SC equation. From the above discussion, it seems that the smallest possible value should always be used. In this study, a value of $C \sim 5\%$ was employed because DES exhibit lower viscosity compared to macromolecules or oligomers, resulting in smaller differences between the viscosity of the pure solvent and the DES + solvent mixture. Consequently, higher concentrations are necessary to ensure a detectable disparity in viscosity upon dilution. Working with small concentrations may reduce the error associated with Eq. C.1, but such small variations would also introduce larger experimental errors related to equipment precision and sample preparation.

The discussion above focused on the error associated with using the SC equation as an approximation of the traditional extrapolation method. To evaluate the sensibility of the calculated $[\eta]$ values to the experimental errors, the system thymol + L-menthol (1:1) (TM0.5) is used for illustration. A sensibility analysis was conducted using SALib Python library [112]. For simplicity, the uncertainty of mass and density measurements was propagated to the concentration. Thus, the inputs to the SC equation function were $C$, $\eta$, and $\eta_0$. The uncertainty of the viscosities was calculated from the variation coefficient of each measurement

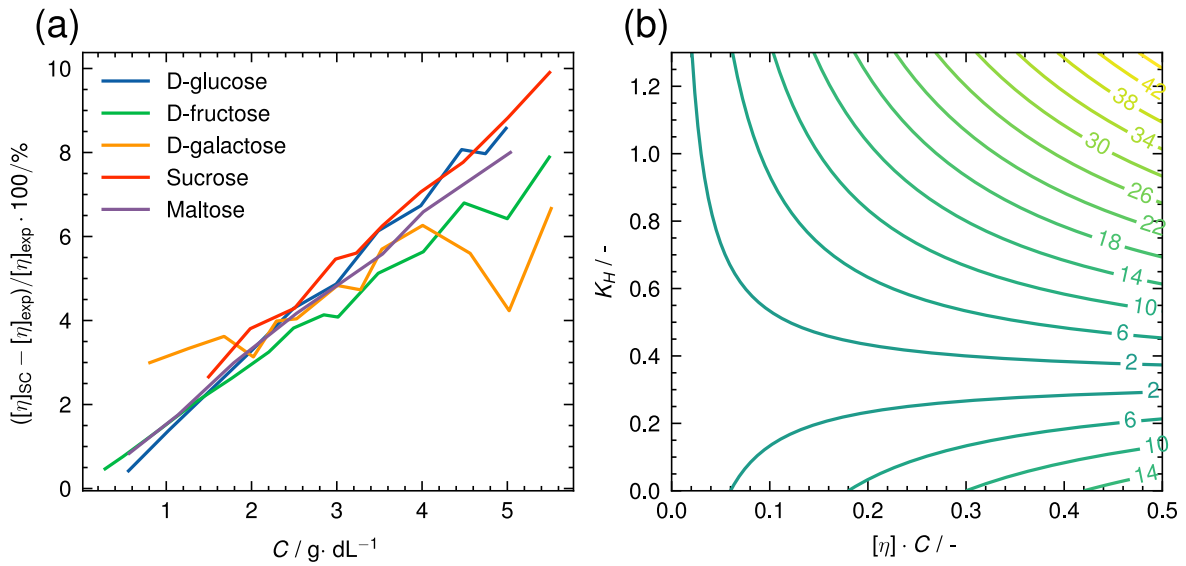


Figure C.1.: Errors associated with the use of the SC equation for calculating the intrinsic viscosity. (a) Relative error of the calculated $[\eta]$ as a function of concentration in various aqueous sugar dilutions; (b) contour lines of the estimated error for $[\eta]$ calculated with Eq. C.1 as a function of the Huggins constant and the product $[\eta]C$.

Table C.1.: Illustration of the sensibility of the experimental error in the calculated intrinsic viscosity for thymol + L-menthol (1:1), using SC equation.

| | | | | | | 1st order Sobol indices / % | | |
|---|---|---|---|---|---|---|---|---|
| Solvent | $C$ / g·dL$^{-1}$ | $\eta$ / mPa·s | $\eta_0$ / mPa·s | $[\eta]$ / dL·g$^{-1}$ | $\sigma_{[\eta]}$ (%) | $C$ | $\eta$ | $\eta_0$ |
| Acetonitrile | 4.370 | 0.3822 | 0.3556 | 0.01671 | 1.68 | 0.07 | 46.23 | 53.31 |
| THF | 4.064 | 0.5113 | 0.4949 | 0.00807 | 2.70 | 0.03 | 48.23 | 51.37 |
| Dichloromethane | 4.660 | 0.4674 | 0.4665 | 0.00042 | 47.00 | 0.00 | 48.84 | 49.97 |
| Methanol | 4.180 | 0.5973 | 0.5540 | 0.01823 | 1.03 | 0.19 | 46.03 | 53.41 |
| Chloroform | 4.243 | 0.5884 | 0.5667 | 0.00891 | 2.04 | 0.05 | 47.97 | 51.61 |
| Ethyl acetate | 4.422 | 0.4771 | 0.4408 | 0.01811 | 1.23 | 0.13 | 45.86 | 53.62 |
| Chorobenzene | 4.548 | 0.7953 | 0.7611 | 0.00974 | 1.30 | 0.11 | 47.62 | 51.89 |
| Acetic anhydride | 4.269 | 0.9129 | 0.8728 | 0.01060 | 1.11 | 0.17 | 47.55 | 51.91 |

given by the rolling-ball viscometer (between $2\cdot10^{-3}$ and $3\cdot10^{-3}$ mPa·s on average). A normal distribution was assumed for each input variable, with the measured value as the mean, and a sample of 1024 datapoints was generated around this mean using the respective standard deviations. The Sobol sensitivity indices were also calculated. These quantify how much of the variance in the model output each uncertain parameter is responsible for. Here, only the first-order Sobol sensitivity indices are shown, which measure the direct effect each parameter has on the variance of the model. Note that although these are expressed as percentages, they do not necessarily sum up 100%, since some contributions may come from combinations between parameters (higher order indices).

The results of the sensibility analysis for the TM0.5 DES are shown in Table C.1. It is ob-

served that the standard deviation values of the calculated $[\eta]$ using SC equation are below 3%, except for the particularly high value for dichloromethane (47%). This is a consequence of the very small change in viscosity upon DES addition to the dichloromethane; $[\eta]$ values are around 2 orders of magnitude lower than in the other solvents. This was observed for dichloromethane in thymol + L-menthol systems, and for 1,4-dioxane in thymol + cyclohexanone systems. Nevertheless, the large deviation, which is relative to a small intrinsic viscosity, does not have a great effect on the HSP calculations. Since the HSP2-S and FSP methods use the intrinsic viscosity values as weights (each $[\eta]$ is divided by the maximum obtained value) the contribution of the solvent to the calculation is negligible, regardless of the deviation. This is not the case for the HSP2-B method which, as mentioned in the manuscript, is more sensitive to small variations. The first order Sobol sensitivity indices show that the variance of the calculated $[\eta]$ is given almost completely by the uncertainty in the viscosities. The standard deviation of the concentration, not the concentration as a variable itself, has practically no effect on the standard deviation of $[\eta]$ when compared to the standard deviation of the viscosities.

Table C.2.: Intrinsic viscosity calculated for thymol + L-menthol at different molar fractions and 298.15 K.

| Thymol molar fraction | Solvent | $\eta$ / mPa·s | $[\eta_i]$ / 100 mL·g$^{-1}$ | Water content / ppm |
|---|---|---|---|---|
| 0.33 | Acetonitrile | 0.3808 | 0.01514 | 1182.2 |
| | THF | 0.5245 | 0.01282 | 1463.4 |
| | Dichloromethane | 0.4768 | 0.00479 | 412.8 |
| | Methanol | 0.6188 | 0.02464 | 2827.0 |
| | Chloroform | 0.606 | 0.01483 | 314.9 |
| | Ethyl acetate | 0.4843 | 0.02090 | 4056.1 |
| | Chlorobenzene | 0.8068 | 0.01287 | 289.8 |
| | Acetic anhydride | 0.9303 | 0.01410 | 42.5 |
| 0.42 | Acetonitrile | 0.3794 | 0.01436 | 1142.8 |
| | THF | 0.5184 | 0.01042 | 1363.0 |
| | Dichloromethane | 0.4615 | 0.00238 | 423.5 |
| | Methanol | 0.5989 | 0.01812 | 2165.0 |
| | Chloroform | 0.5942 | 0.01017 | 256.6 |
| | Ethyl acetate | 0.472 | 0.01525 | 4038.0 |
| | Chlorobenzene | 0.7935 | 0.00963 | 223.5 |
| | Acetic anhydride | 0.9122 | 0.01040 | 200.7 |
| 0.5 | Acetonitrile | 0.3822 | 0.01671 | 784.2 |
| | THF | 0.5113 | 0.00807 | 1306.5 |
| | Dichloromethane | 0.4674 | 0.00041 | 395.9 |
| | Methanol | 0.5973 | 0.01823 | 2095.6 |
| | Chloroform | 0.5884 | 0.00891 | 219.7 |
| | Ethyl acetate | 0.47705 | 0.01811 | 4347.5 |
| | Chlorobenzene | 0.7953 | 0.00974 | 245.2 |
| | Acetic anhydride | 0.9129 | 0.01060 | 126.0 |
| 0.59 | Acetonitrile | 0.374 | 0.01117 | 1148.2 |
| | THF | 0.5192 | 0.01097 | 1880.7 |
| | Dichloromethane | 0.4661 | 0.00018 | 478.2 |
| | Methanol | 0.6066 | 0.01928 | 2970.4 |
| | Chloroform | 0.5937 | 0.01018 | 332.4 |
| | Ethyl acetate | 0.4739 | 0.01638 | 4163.6 |
| | Chlorobenzene | 0.7943 | 0.00946 | 302.2 |
| | Acetic anhydride | 0.919 | 0.01156 | 227.6 |
| 0.67 | Acetonitrile | 0.3739 | 0.01104 | 701.0 |
| | THF | 0.5171 | 0.01055 | 1888.6 |
| | Dichloromethane | 0.4716 | 0.00228 | 381.2 |
| | Methanol | 0.596 | 0.01790 | 2180.5 |
| | Chloroform | 0.592 | 0.00958 | 239.4 |
| | Ethyl acetate | 0.4739 | 0.01693 | 4178.6 |
| | Chlorobenzene | 0.7911 | 0.00941 | 256.4 |
| | Acetic anhydride | 0.9192 | 0.01207 | 170.2 |

Table C.3.: Intrinsic viscosity calculated for thymol + cyclohexanone at different molar fractions and 298.15 K.

| Thymol molar fraction | Solvent | $\eta$ / mPa·s | $[\eta_i]$ / 100 mL·g$^{-1}$ |
|---|---|---|---|
| 0.05 | Acetonitrile | 0.3694 | 0.00835 |
| | THF | 0.5026 | 0.00329 |
| | Dioxane | 1.2018 | 0.00286 |
| | Methanol | 0.5743 | 0.00765 |
| | Chloroform | 0.6041 | 0.01388 |
| | Ethyl acetate | 0.4654 | 0.01184 |
| | DMSO | 2.0598 | 0.00611 |
| | Acetic anhydride | 0.8965 | 0.00599 |
| 0.1 | Acetonitrile | 0.3805 | 0.01494 |
| | THF | 0.5106 | 0.00681 |
| | Dioxane | 1.2076 | 0.00179 |
| | Methanol | 0.5787 | 0.01032 |
| | Chloroform | 0.6053 | 0.01473 |
| | Ethyl acetate | 0.4658 | 0.01187 |
| | DMSO | 2.0722 | 0.00484 |
| | Acetic anhydride | 0.9001 | 0.00680 |
| 0.2 | Acetonitrile | 0.3718 | 0.00995 |
| | THF | 0.506 | 0.00471 |
| | Dioxane | 1.216 | 0.00027 |
| | Methanol | 0.5798 | 0.00962 |
| | Chloroform | 0.5995 | 0.01183 |
| | Ethyl acetate | 0.4686 | 0.01332 |
| | DMSO | 2.0954 | 0.00241 |
| | Acetic anhydride | 0.9058 | 0.00806 |
| 0.5 | Acetonitrile | 0.3764 | 0.01258 |
| | THF | 0.5152 | 0.00865 |
| | Dioxane | 1.2467 | 0.00524 |
| | Methanol | 0.593 | 0.01501 |
| | Chloroform | 0.6011 | 0.01227 |
| | Ethyl acetate | 0.4724 | 0.01527 |
| | DMSO | 2.1468 | 0.00291 |
| | Acetic anhydride | 0.9401 | 0.01641 |
| 0.7 | Acetonitrile | 0.3826 | 0.01601 |
| | THF | 0.5167 | 0.00944 |
| | Dioxane | 1.2592 | 0.00746 |
| | Methanol | 0.5954 | 0.01561 |
| | Chloroform | 0.5948 | 0.01039 |
| | Ethyl acetate | 0.4782 | 0.01807 |
| | DMSO | 2.1748 | 0.00590 |
| | Acetic anhydride | 0.9165 | 0.01082 |

Table C.4.: Viscosity of the solvents used for intrinsic viscosity calculations. Data gathered at 298.15 K

| | $\eta$ [mPa·s] | |
|---|---|---|
| Solvent | This work | Literature |
| Acetonitrile | 0.3556 | 0.344 [113] |
| THF | 0.4949 | 0.463 [113] |
| Dichloromethane | 0.4665 | 0.406 [113] |
| Methanol | 0.554 | 0.550 [113] |
| Chloroform | 0.5667 | 0.5418 [114] |
| Ethyl acetate | 0.4408 | 0.430 [113] |
| Chlorobenzene | 0.7611 | 0.763 [113] |
| Acetic anhydride | 0.8728 | 0.843[115] |
| 1,4-Dioxane | 1.2175 | 1.178 [113] |
| DMSO | 2.1187 | 1.989 [113] |

# D. Bootstrapping

In a general sense, and in the context of the present study, the process of bootstrapping may be summarized [116]. When presented with a set of experimental data, which is used to calculate certain indicator, bootstrapping involves(i) generating a new dataset, known as bootstrap samples, using the same experimental data; (ii) calculating the desired indicator based on the bootstrapped dataset; and (iii) tracking that indicator. This process is then repeated multiple times to estimate a distribution of the calculated indicator. In the present study, this process is utilized to explore the sensitivity of two of the methods used to calculate the HSP from intrinsic viscosity data, HSP2-S and HSP2-B. The procedure goes as follows:

1. For each sample, i.e. each molar fraction of the respective HBA:HBD system, there are measured values of mass, density, and viscosity. Hence, it is considered that these 3 variables add uncertainty to the solubility parameter calculation.

2. As each measured quantity is obtained by using digital equipment with high accuracy, it is assumed that the measured value corresponds to a hypothetical mean of a normal distribution of values.

3. Each column (e.g. solvent viscosity, density, solvent mass, etc) is resampled, that is, each value is used as the mean to randomly generate another value using NumPy library in Python, with the scale parameter corresponding to the standard deviation of each column (e.g. a mass column would have the precision of the analytical balance), and a size of 10000. Then, from the random values generated, one is randomly picked.

4. Both methods, HSP2-S and HSP2-B, are employed to calculate the HSP using the bootstrapped values.

5. This process is repeated 500 times.

This procedure allows to assign a standard deviation to each HSP, which reflects the variability in the HSP estimates due to the uncertainty in the measured variables. In this way, it is possible to calculate the standard deviation lines for HSP2-B and HSP2-S shown in Fig. 3 of the main document. It should be noted that this procedure is not applicable to the HSP1 method, as the inputs are binary (1 or 0). Regarding the FSP method, the developers of this method implemented specific metrics of reliability in the FreeFEM++ code described in the original work [61]. These involve characteristics of the tetrahedra obtained from the triangulation.

# E. PC-SAFT parameters

Table E.1.: Total volume and surface area of the cavity obtained from ORCA, along with PC-SAFT parameters for the solid compounds and solvents calcualted in this work.

| Compound | $V$ / bohr$^3$ | $A$ / bohr$^2$ | $m_i$ / - | $\sigma_{ii}$ / Å | $\epsilon_{ii}/k$ / K | $\epsilon^{A_iB_i}/k$ / K |
|---|---|---|---|---|---|---|
| *Solids:* | | | | | | |
| 2-Chlorobenzoic acid | 1102.40 | 622.85 | 1.76 | 5.62 | 345.36 | 2181.94 |
| 3-Chlorobenzoic acid | 1104.38 | 626.86 | 1.79 | 5.59 | 343.94 | 2189.21 |
| Acridine | 1441.54 | 759.70 | 1.87 | 6.02 | 362.70 | 2093.61 |
| Ascorbic Acid | 1178.52 | 681.11 | 2.01 | 5.49 | 337.97 | 2219.60 |
| Benzamide | 994.57 | 572.19 | 1.67 | 5.52 | 339.54 | 2211.61 |
| Benzoic acid | 964.12 | 555.87 | 1.63 | 5.51 | 338.80 | 2215.36 |
| Borneol | 1349.91 | 723.62 | 1.84 | 5.92 | 359.11 | 2111.91 |
| Caffeine | 1420.21 | 779.83 | 2.08 | 5.78 | 353.36 | 2141.21 |
| Curcumin | 2827.04 | 1519.14 | 3.88 | 5.91 | 358.56 | 2114.71 |
| Dapsone | 1820.70 | 983.52 | 2.54 | 5.88 | 357.36 | 2120.83 |
| d-Camphor | 1309.23 | 705.31 | 1.81 | 5.89 | 357.98 | 2117.63 |
| D-xylose | 1033.80 | 604.92 | 1.83 | 5.43 | 333.48 | 2242.48 |
| Glycine | 575.69 | 377.12 | 1.43 | 4.85 | 272.78 | 2551.76 |
| Ibuprofen | 1774.10 | 988.07 | 2.71 | 5.70 | 349.56 | 2160.58 |
| Ketoprofen | 2008.79 | 1071.51 | 2.70 | 5.95 | 360.19 | 2106.41 |
| L-Menthol | 1434.51 | 797.27 | 2.18 | 5.71 | 350.13 | 2157.63 |
| Monuron | 1510.82 | 836.42 | 2.27 | 5.73 | 351.20 | 2152.20 |
| Paracetamol | 1196.11 | 683.51 | 1.97 | 5.56 | 341.78 | 2200.17 |
| Perylene | 1976.25 | 970.95 | 2.07 | 6.46 | 374.19 | 2035.07 |
| Phenol | 798.72 | 471.32 | 1.45 | 5.38 | 330.23 | 2259.03 |
| Quercetin | 2006.87 | 1047.61 | 2.52 | 6.08 | 364.56 | 2084.14 |
| Salicylic acid | 1012.18 | 575.99 | 1.65 | 5.58 | 343.13 | 2193.30 |
| Succinic acid | 854.82 | 529.80 | 1.80 | 5.12 | 307.66 | 2374.04 |
| Thymol | 1332.24 | 752.54 | 2.12 | 5.62 | 345.43 | 2181.57 |
| *Liquids:* | | | | | | |
| 1,2-Propanediol | 660.25 | 425.96 | 1.57 | 4.92 | 283.59 | 2496.69 |
| 1-Butanol | 726.85 | 462.08 | 1.65 | 4.99 | 293.09 | 2448.29 |
| Acetonitrile | 425.68 | 293.88 | 1.24 | 4.60 | 227.10 | 2784.53 |
| Cyclohexanone | 865.38 | 511.01 | 1.58 | 5.38 | 329.96 | 2260.43 |
| Ethanol | 459.73 | 318.27 | 1.35 | 4.59 | 224.27 | 2798.97 |
| Ethyl acetate | 767.37 | 486.18 | 1.73 | 5.01 | 295.18 | 2437.64 |
| Hexane | 947.02 | 590.02 | 2.03 | 5.10 | 304.85 | - |
| Limonene | 1300.72 | 727.95 | 2.02 | 5.67 | 348.18 | 2167.59 |

# F. Solids properties

Table F.1.: Thermal properties of selected solutes for solubility calculation.

| Chemical | CAS | $M_w$ / g·mol$^{-1}$ | $T_m$ / K | $\Delta H_m$ / kJ·mol$^{-1}$ |
|---|---|---|---|---|
| 2-Chlorobenzoic acid | 118-91-2 | 156.57 | 414.0[117] | 25.25[117] |
| 2-Methylbenzoic acid | 118-90-1 | 136.15 | 376.9[118] | 20.2[118] |
| 3,5-Dinitrobenzoic acid | 99-34-3 | 212.12 | 480.4[119] | 22.8[119] |
| 3-Chlorobenzoic acid | 535-80-8 | 156.57 | 427.4[118] | 23.9[118] |
| 3-Methylbenzoic acid | 99-04-7 | 136.15 | 381.9[118] | 15.7[118] |
| 3-Nitrobenzoic acid | 121-92-6 | 167.12 | 414.3[120] | 19.3[120] |
| Acridine | 260-94-6 | 179.22 | 383.2[121] | 20.7[121] |
| Adipic acid | 124-04-9 | 146.14 | 419.0[122] | 33.7[122] |
| Ascorbic Acid | 50-81-7 | 176.12 | 465.15[123] | 29.2[123] |
| Benzamide | 55-21-0 | 121.14 | 400.4[115] | 19.5[115] |
| Benzoic acid | 65-85-0 | 122.12 | 395.5[124] | 18.0[124] |
| Borneol | 464-45-9 | 154.25 | 480.3[125] | 7.3[125] |
| Caffeine | 58-08-2 | 194.19 | 508.7[126] | 19.6[126] |
| Curcumin | 458-37-7 | 368.38 | 453.4[127] | 47.3[128] |
| Dapsone | 80-08-0 | 248.30 | 454.41[129] | 28.62[129] |
| d-Camphor | 464-49-3 | 152.23 | 451.0[130] | 6.2[130] |
| Diclofenac | 15307-86-5 | 296.15 | 452.6[131] | 40.4[131] |
| D-Xylose | 10257-31-5 | 150.13 | 416.2[132] | 31.7[132] |
| Glutaric acid | 110-94-1 | 132.11 | 370.9[133] | 20.7[133] |
| Glycine | 56-40-6 | 75.07 | 569.0[134] | 21.0[134] |
| Ibuprofen | 15687-27-1 | 206.29 | 350.4[135] | 39.5[135] |
| Ketoprofen | 22071-15-4 | 254.28 | 368.0[136] | 37.3[136] |
| L-Menthol | 2216-51-5 | 156.27 | 315.7[137] | 12.9[137] |
| Monuron | 150-68-5 | 198.65 | 447.6[138] | 29.3[138] |
| Naproxen | 22204-53-1 | 230.26 | 428.8[136] | 34.2[136] |
| p-Aminobenzoic acid | 150-13-0 | 137.14 | 458.7[139] | 22.6[139] |
| Paracetamol | 103-90-2 | 151.16 | 443.2[140] | 27.6[140] |
| Perylene | 198-55-0 | 252.30 | 551.0[118] | 31.9[118] |
| Phenol | 108-95-2 | 94.11 | 314.0[141] | 11.5[141] |
| Quercetin | 117-39-5 | 302.24 | 589.6[41] | 41.5[142] |
| Salicylic acid | 69-72-7 | 138.12 | 432.5[143] | 23.1[143] |
| Succinic acid | 110-15-6 | 118.09 | 460.2[144] | 33.0[144] |
| Thymol | 89-83-8 | 150.22 | 323.5[137] | 19.6[137] |

# G. Experimental solubility of solids in pure solvents

Table G.1.: Experimental solubility values obtained from literature, along with the predictions from each model.

| Solute | Solvent | Literature | $T$ / K | FH-HSP | openCOSMO-RS | PC-SAFT |
|---|---|---|---|---|---|---|
| L-menthol | Acetonitrile | 0.4047[145] | 298.15 | 0.7417 | 0.3791 | 0.7454 |
| L-menthol | 1-Butanol | 0.7103[145] | 298.15 | 0.7415 | 0.7446 | 0.7503 |
| L-menthol | Ethanol | 0.6510[145] | 298.15 | 0.7459 | 0.7396 | 0.7479 |
| L-menthol | Ethyl acetate | 0.6805[145] | 298.15 | 0.7429 | 0.7644 | 0.7509 |
| L-menthol | Hexane | 0.6927[145] | 298.15 | 0.6591 | 0.7275 | 0.7365 |
| L-menthol | R-Limonene | 0.6906[145] | 298.15 | 0.7122 | 0.7278 | 0.7490 |
| L-menthol | 1,2-Propanediol | 0.6179[145] | 298.15 | 0.7308 | 0.7024 | 0.7498 |
| Thymol | Acetonitrile | 0.7059[145] | 298.15 | 0.5731 | 0.6958 | 0.5345 |
| Thymol | 1-Butanol | 0.6663[145] | 298.15 | 0.5743 | 0.7117 | 0.5416 |
| Thymol | Ethanol | 0.6586[145] | 298.15 | 0.5912 | 0.6931 | 0.5407 |
| Thymol | Ethyl acetate | 0.7090[145] | 298.15 | 0.5730 | 0.7590 | 0.5429 |
| Thymol | Hexane | 0.3380[145] | 298.15 | 0.1805 | 0.3709 | 0.4715 |
| Thymol | R-Limonene | 0.4797[145] | 298.15 | 0.5148 | 0.4681 | 0.5372 |
| Thymol | 1,2-Propanediol | 0.6959[145] | 298.15 | 0.5481 | 0.7325 | 0.5413 |
| 2-Methylbenzoic acid | Cyclohexanone | 0.2045[146] | 298.2 | 0.1533 | 0.4994 | 0.4287 |
| 3,5-Dinitrobenzoic acid | Cyclohexanone | 0.1402[146] | 298.2 | 0.0107 | 0.3624 | 0.1713 |
| 3-Methylbenzoic acid | Cyclohexanone | 0.1789[146] | 298.2 | 0.2149 | 0.5256 | 0.4982 |
| 3-Nitrobenzoic acid | Cyclohexanone | 0.1904[146] | 298.2 | 0.0691 | 0.4534 | 0.3340 |
| Adipic acid | Cyclohexanone | 0.0148[147] | 298.75 | 0.0089 | 0.1479 | 0.1394 |
| Benzoic acid | Cyclohexanone | 0.2363[146] | 298.2 | 0.1351 | 0.4648 | 0.4094 |
| Glutaric acid | Cyclohexanone | 0.1891[148] | 299.7 | 0.1375 | 0.3847 | 0.4478 |
| Succinic acid | Cyclohexanone | 0.01131[144] | 298.55 | 0.0057 | 0.1632 | 0.0976 |

# H. Calculated HSP

Table H.1.: Summary of the HSP calculated for thymol + cyclohexanone (TC) and thymol + L-menthol (TM) with each method. Calculated at 298.15 K and 1 atm. — indicates that the regression was not able to adjust a feasible value. HSP of the pure compounds were retrieved from [1].

| | | HSP1 | | | HSP2-S | | | HSP2-B | | | FSP | | |
|---|---|---|---|---|---|---|---|---|---|---|---|---|---|
| DES | Molar fraction | $\delta_d$ | $\delta_p$ | $\delta_h$ | $\delta_d$ | $\delta_p$ | $\delta_h$ | $\delta_d$ | $\delta_p$ | $\delta_h$ | $\delta_d$ | $\delta_p$ | $\delta_h$ |
| | 0.0 | 16.60 | 4.70 | 10.60 | 16.60 | 4.70 | 10.60 | 16.60 | 4.70 | 10.60 | 16.60 | 4.70 | 10.60 |
| | 0.33 | 16.90 | 9.90 | 8.50 | 16.29 | 8.79 | 9.80 | 16.81 | 13.31 | 13.69 | 16.18 | 9.57 | 9.92 |
| | 0.42 | 17.30 | 7.80 | 13.30 | 16.26 | 8.95 | 9.77 | 16.86 | 12.97 | 13.27 | 16.16 | 9.69 | 9.88 |
| TM | 0.5 | 17.70 | 9.50 | 12.30 | 16.17 | 9.33 | 9.81 | 16.91 | 12.96 | 12.68 | 16.13 | 9.80 | 9.85 |
| | 0.59 | 17.30 | 7.80 | 13.30 | 16.21 | 8.63 | 10.30 | 16.78 | 13.93 | 13.37 | 16.14 | 9.64 | 10.06 |
| | 0.67 | 17.50 | 9.30 | 12.30 | 16.23 | 8.67 | 10.15 | 16.89 | 13.29 | 13.21 | 16.16 | 9.61 | 9.94 |
| | 1.0 | 19.00 | 4.50 | 10.80 | 19.00 | 4.50 | 10.80 | 19.00 | 4.50 | 10.80 | 19.00 | 4.50 | 10.80 |
| | 0.0 | 17.80 | 6.30 | 5.10 | 17.80 | 6.30 | 5.10 | 17.80 | 6.30 | 5.10 | 17.80 | 6.30 | 5.10 |
| | 0.05 | 16.10 | 7.50 | 11.70 | 16.47 | 9.46 | 9.40 | — | — | — | 16.36 | 11.01 | 10.82 |
| | 0.1 | 16.29 | 7.59 | 11.71 | 16.23 | 10.07 | 9.47 | 16.83 | 10.08 | 18.52 | 16.30 | 11.19 | 10.75 |
| TC | 0.2 | 17.00 | 6.90 | 10.00 | 16.23 | 9.11 | 9.50 | 16.92 | 10.46 | 17.32 | 16.23 | 11.08 | 10.94 |
| | 0.5 | 13.90 | 10.90 | 10.50 | 16.02 | 9.75 | 10.33 | 15.88 | 10.37 | 14.68 | 16.25 | 10.99 | 11.15 |
| | 0.7 | 15.80 | 7.90 | 11.40 | 16.13 | 10.19 | 10.08 | — | — | — | 16.28 | 11.00 | 11.06 |
| | 1.0 | 19.00 | 4.50 | 10.80 | 19.00 | 4.50 | 10.80 | 19.00 | 4.50 | 10.80 | 19.00 | 4.50 | 10.80 |

# I. openCOSMO-RS benchmark

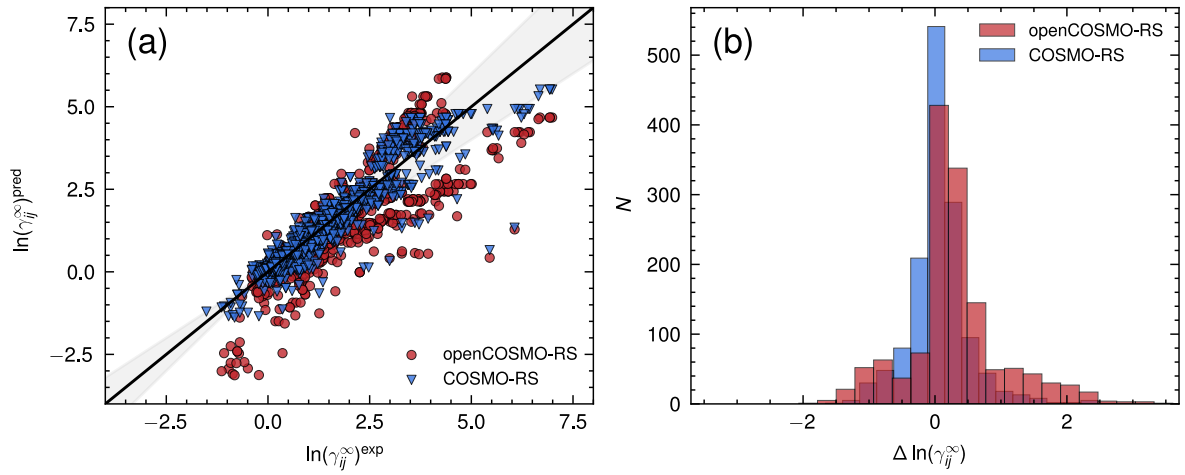


Figure I.1.: Predictions obtained with openCOSMO-RS over the experimental data and COSMO-RS predictions. (a) parity plot of the predictions, where the solid line indicates perfect predictions, and the gray band indicates a relative deviation of ±20% ; (b) histogram of the differences of the predictions for $\ln \gamma_{ij}^{\infty}$ with the openCOSMO-RS, COSMO-RS and the corresponding experimental values (exp) from [67]. $\Delta \ln \gamma_{ij}^{\infty} = \ln \gamma_{ij}^{\infty\text{pred}} - \ln \gamma_{ij}^{\infty\text{exp}}$. $N$ represents the number of binary mixtures $ij$ for which the differences are within the given intervals.